EUROPEAN ORGANIZATION FOR NUCLEAR RESEARCH (CERN)

CERN-PH-EP/2011-170
2013/04/30

CMS-HIN-10-006

Suppression of non-prompt J/ψ, prompt J/ψ, and Υ(1S) in PbPb collisions at $\sqrt{s_{\mathrm{NN}}} = 2.76\,\mathrm{TeV}$

The CMS Collaboration*

Abstract

Yields of prompt and non-prompt J/ψ, as well as Υ(1S) mesons, are measured by the CMS experiment via their $\mu^+\mu^-$ decays in PbPb and pp collisions at $\sqrt{s_{\mathrm{NN}}} = 2.76\,\mathrm{TeV}$ for quarkonium rapidity $|y| < 2.4$. Differential cross sections and nuclear modification factors are reported as functions of y and transverse momentum p_{T}, as well as collision centrality. For prompt J/ψ with relatively high p_{T} ($6.5 < p_{\mathrm{T}} < 30\,\mathrm{GeV}/c$), a strong, centrality-dependent suppression is observed in PbPb collisions, compared to the yield in pp collisions scaled by the number of inelastic nucleon-nucleon collisions. In the same kinematic range, a suppression of non-prompt J/ψ, which is sensitive to the in-medium b-quark energy loss, is measured for the first time. Also the low-p_{T} Υ(1S) mesons are suppressed in PbPb collisions.

Submitted to the Journal of High Energy Physics

*See Appendix B for the list of collaboration members

1 Introduction

At large energy densities and high temperatures, strongly interacting matter consists of a deconfined and chirally-symmetric system of quarks and gluons [1]. This state, often referred to as "quark-gluon plasma" (QGP) [2], constitutes the main object of the studies performed with relativistic heavy-ion collisions [3–6].

The formation of a QGP in high-energy nuclear collisions can be evidenced in a variety of ways. One of its most striking expected signatures is the suppression of quarkonium states [7], both of the charmonium (J/ψ, ψ', χ_c, etc.) and the bottomonium (Y(1S, 2S, 3S), χ_b, etc.) families. This is thought to be a direct effect of deconfinement, when the binding potential between the constituents of a quarkonium state, a heavy quark and its antiquark, is screened by the colour charges of the surrounding light quarks and gluons. The suppression is predicted to occur above the critical temperature of the medium (T_c) and depends on the $\mathrm{Q\overline{Q}}$ binding energy. Since the Y(1S) is the most tightly bound state among all quarkonia, it is expected to be the one with the highest dissociation temperature. Examples of dissociation temperatures are given in Ref. [8]: $T_{\mathrm{dissoc}} \sim 1\,T_c$, $1.2\,T_c$, and $2\,T_c$ for the Y(3S), Y(2S), and Y(1S), respectively. Similarly, in the charmonium family the dissociation temperatures are $\leq 1\,T_c$ and $1.2\,T_c$ for the ψ' and J/ψ, respectively. However, there are further possible changes to the quarkonium production in heavy-ion collisions. On the one hand, modifications to the parton distribution functions inside the nucleus (shadowing) and other cold-nuclear-matter effects can reduce the production of quarkonia without the presence of a QGP [9, 10]. On the other hand, the large number of heavy quarks produced in heavy-ion collisions, in particular at the energies accessible by the Large Hadron Collider (LHC), could lead to an increased production of quarkonia via statistical recombination [11–16].

Charmonium studies in heavy-ion collisions have been carried out for 25 years, first at the Super Proton Synchrotron (SPS) by the NA38 [17], NA50 [18, 19], and NA60 [20] fixed-target experiments at 17.3–19.3 GeV centre-of-mass energy per nucleon pair ($\sqrt{s_{\mathrm{NN}}}$), and then at the Relativistic Heavy Ion Collider (RHIC) by the PHENIX experiment at $\sqrt{s_{\mathrm{NN}}} = 200$ GeV [21]. In all cases, J/ψ suppression was observed in the most central collisions. At the SPS, the suppression of the ψ' meson was also measured [19]. Experimentally, the suppression is quantified by the ratio of the yield measured in heavy-ion collisions and a reference. At RHIC, the reference was provided by the properly scaled yield measured in pp collisions. Such a ratio is called the nuclear modification factor, R_{AA}. In the absence of modifications, one would expect $R_{AA} = 1$ for hard processes, which scale with the number of inelastic nucleon-nucleon collisions. For bottomonia, the production cross section is too small at RHIC to make definitive statements [22]. With the higher energy and luminosity available at the LHC, new studies for charmonia and bottomonia have become possible: (i) ATLAS has reported a suppression of inclusive J/ψ with high transverse momenta p_{T} in central PbPb collisions compared to peripheral collisions at $\sqrt{s_{\mathrm{NN}}} = 2.76$ TeV [23]; (ii) ALICE has measured the R_{AA} for inclusive J/ψ with low p_{T} and sees no centrality dependence of the J/ψ suppression [24]; (iii) a suppression of the excited Y states with respect to the ground state has been observed in PbPb collisions at $\sqrt{s_{\mathrm{NN}}} = 2.76$ TeV compared to pp collisions at the same centre-of-mass energy by the Compact Muon Solenoid (CMS) collaboration [25].

At LHC energies, the inclusive J/ψ yield contains a significant non-prompt contribution from b-hadron decays [26–28]. Owing to the long lifetime of the b hadrons ($\mathcal{O}(500)\,\mu\mathrm{m}/c$), compared to the QGP lifetime ($\mathcal{O}(10)\,\mathrm{fm}/c$), this contribution should not suffer from colour screening, but instead may reflect the b-quark energy loss in the medium. Such energy loss would lead to a reduction of the b-hadron yield at high p_{T} in PbPb collisions compared to the binary-collision-

scaled pp yield. In heavy-ion collisions, only indirect measurements of this effect exist, through single electrons from semileptonic open heavy-flavour decays [29–31]; to date, the contributions from charm and bottom have not been disentangled. The importance of an unambiguous measurement of open bottom flavour is driven by the lack of knowledge regarding key features of the dynamics of parton energy loss in the QGP, such as its colour-charge and parton-mass dependencies [32, 33] and the relative role of radiative and collisional energy loss [34]. CMS is well equipped to perform direct measurements of b-hadron production in heavy-ion collisions by identifying non-prompt J/ψ from b-hadron decays via the reconstruction of secondary $\mu^+\mu^-$ vertices.

The paper is organised as follows: the CMS detector is briefly described in Section 2. Section 3 presents the data collection, the PbPb event selection, the muon reconstruction and selection, and the Monte Carlo (MC) simulations. The methods employed for signal extraction are detailed in Section 4. Section 5 describes the acceptance correction factors and the estimation of the reconstruction efficiencies. The pp baseline measurements are summarized in Section 6. The results are presented in Section 7, followed by their discussion in Section 8.

2 The CMS Detector

A detailed description of the CMS experiment can be found in Ref. [35]. The central feature of the CMS apparatus is a superconducting solenoid of 6 m internal diameter. Within the field volume are the silicon tracker, the crystal electromagnetic calorimeter, and the brass/scintillator hadron calorimeter.

CMS uses a right-handed coordinate system, with the origin at the nominal interaction point, the x axis pointing to the centre of the LHC, the y axis pointing up (perpendicular to the LHC plane), and the z axis along the counterclockwise-beam direction. The polar angle θ is measured from the positive z axis and the azimuthal angle ϕ is measured in the x-y plane. The pseudorapidity is defined as $\eta = -\ln[\tan(\theta/2)]$.

Muons are detected in the interval $|\eta| < 2.4$ by gaseous detectors made of three technologies: drift tubes, cathode strip chambers, and resistive plate chambers, embedded in the steel return yoke. The silicon tracker is composed of pixel detectors (three barrel layers and two forward disks on either side of the detector, made of 66 million $100 \times 150\,\mu\text{m}^2$ pixels) followed by microstrip detectors (ten barrel layers plus three inner disks and nine forward disks on either side of the detector, with strips of pitch between 80 and 180 μm). The transverse momentum of muons matched to reconstructed tracks is measured with a resolution better than $\sim$1.5% for p_{T} smaller than 100 GeV/c [36]. The good resolution is the result of the 3.8 T magnetic field and the high granularity of the silicon tracker.

In addition, CMS has extensive forward calorimetry, including two steel/quartz-fibre Cherenkov forward hadron (HF) calorimeters, which cover the pseudorapidity range $2.9 < |\eta| < 5.2$. These detectors are used in the present analysis for the event selection and PbPb collision centrality determination, as described in the next section. Two beam scintillator counters (BSC) are installed on the inner side of the HF calorimeters for triggering and beam-halo rejection.

3 Data Selection

3.1 Event Selection

Inelastic hadronic PbPb collisions are selected using information from the BSC and HF calorimeters, in coincidence with a bunch crossing identified by the beam pick-up (one on each side of the interaction point) [35]. Events are further filtered offline by requiring a reconstructed primary vertex based on at least two tracks, and at least 3 towers on each HF with an energy deposit of more than 3 GeV per tower. These criteria reduce contributions from single-beam interactions with the environment (e.g. beam-gas collisions and collisions of the beam halo with the beam pipe), ultra-peripheral electromagnetic interactions, and cosmic-ray muons. A small fraction of the most peripheral PbPb collisions are not selected by these *minimum-bias* requirements, which accept $(97 \pm 3)\%$ of the inelastic hadronic cross section [37]. A sample corresponding to 55.7 M minimum-bias events passes all these filters. Assuming an inelastic PbPb cross section of $\sigma_{\mathrm{PbPb}} = 7.65$ b [37], this sample corresponds to an integrated luminosity of $\mathcal{L}_{\mathrm{int}} = 7.28\,\mu\mathrm{b}^{-1}$. This value is only mentioned for illustration purposes; the final results are normalized to the number of minimum-bias events.

The measurements reported here are based on dimuon events triggered by the Level-1 (L1) trigger, a hardware-based trigger that uses information from the muon detectors. The CMS detector is also equipped with a software-based high-level trigger (HLT). However, no further requirements at the HLT level have been applied to the L1 muon objects used for this analysis.

The event centrality distribution of minimum-bias events is compared to events selected by the double-muon trigger in Fig. 1. The centrality variable is defined as the fraction of the total cross section, starting at 0% for the most central collisions. This fraction is determined from the distribution of total energy measured in both HF calorimeters [38]. Using a Glauber-model calculation as described in Ref. [37], one can estimate variables related to the centrality, such as the number of nucleons participating in the collisions (N_{part}) and the nuclear overlap function (T_{AA}), which is equal to the number of elementary nucleon-nucleon (NN) binary collisions divided by the elementary NN cross section and can be interpreted as the NN equivalent integrated luminosity per heavy ion collision, at a given centrality [39]. The values of these variables are presented in Table 1 for the centrality bins used in this analysis. The double-muon-triggered events are more frequent in central collisions since the main physics processes that generate high-p_{T} muon pairs scale with the number of inelastic nucleon-nucleon collisions. In the following, N_{part} will be the variable used to show the centrality dependence of the measurements.

Simulated MC events are used to tune the muon selection criteria, to compute the acceptance and efficiency corrections, and to obtain templates of the decay length distribution of J/ψ from b-hadron decays. For the acceptance corrections described in Section 5.1, three separate MC samples, generated over full phase space, are used: prompt J/ψ, J/ψ from b-hadron decays, and $\Upsilon(1\mathrm{S})$. Prompt J/ψ and $\Upsilon(1\mathrm{S})$ are produced using PYTHIA 6.424 [40] at $\sqrt{s} = 2.76$ TeV, which generates events based on the leading-order colour-singlet and colour-octet mechanisms, with non-relativistic quantum chromodynamics (QCD) matrix elements tuned [41] by comparison with CDF data [42]. The colour-octet states undergo a shower evolution. For the non-prompt J/ψ studies, the b-hadron events are produced with PYTHIA in generic QCD $2\to2$ processes. In all three samples, the J/ψ or $\Upsilon(1\mathrm{S})$ decay is simulated using the EVTGEN [43] package. Prompt J/ψ and $\Upsilon(1\mathrm{S})$ are simulated assuming unpolarized production, while the non-prompt J/ψ polarization is determined by the sum of the exclusive states generated by EVTGEN. Final-state bremsstrahlung is implemented using PHOTOS [44].

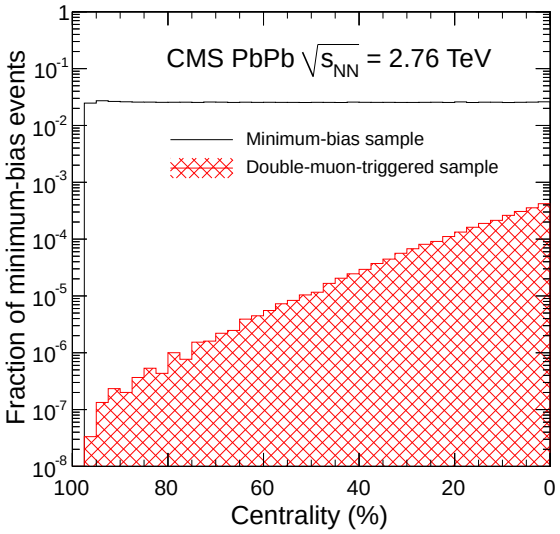

Figure 1: Centrality distribution of the minimum-bias sample (solid black line) overlaid with the double-muon triggered sample (hashed red) in bins of 2.5%.

Table 1: Average and root-mean-square (RMS) values of the number of participating nucleons (N_{part}) and of the nuclear overlap function (T_{AA}) for the centrality bins used in this analysis [37].

	N_{part}		T_{AA} (mb^{-1})	
Centrality (%)	Mean	RMS	Mean	RMS
0–10	355.4	33.3	23.19	3.77
10–20	261.4	30.4	14.48	2.86
20–30	187.2	23.4	8.78	1.94
30–40	130.0	17.9	5.09	1.27
40–50	86.3	13.6	2.75	0.80
50–100	22.1	19.3	0.47	0.54
0–20	308.4	56.8	18.83	5.49
20–100	64.2	63.0	2.37	3.05
0–100	113.1	115.6	5.66	7.54

For some MC simulation studies, in particular the efficiency corrections described in Section 5.2, the detector response to each PYTHIA signal event is simulated with GEANT4 [45] and then embedded in a realistic heavy-ion background event. The background events are produced with the HYDJET event generator [46] and then simulated with GEANT4 as well. The HYDJET parameters were tuned to reproduce the particle multiplicities at all centralities seen in data. The embedding is done at the level of detector hits and requires that the signal and background production vertices match. The embedded event is then processed through the trigger emulation and the full event reconstruction chain. Collision data are used to validate the efficiencies evaluated using MC simulations, as discussed in Section 5.2.

3.2 Muon Selection

The muon offline reconstruction algorithm starts by reconstructing tracks in the muon detectors, called *standalone muons*. These tracks are then matched to tracks reconstructed in the silicon tracker by means of an algorithm optimized for the heavy-ion environment [47, 48]. The final muon objects, called *global muons*, result from a global fit of the standalone muon and tracker tracks. These are used to obtain the results presented in this paper.

In Fig. 2, the single-muon reconstruction efficiency from MC simulations is presented as a function of the muon p_{T}^{μ} and η^{μ}. The reconstruction efficiency is defined as the number of all reconstructed global muons divided by the number of generated muons in a given (η^{μ}, p_{T}^{μ}) bin. It takes into account detector resolution effects, i.e. reconstructed p_{T} and η values are used in the numerator and generated p_{T} and η values in the denominator. To obtain a clear separation between acceptance and efficiency corrections, a *detectable* single-muon acceptance is defined in the (η^{μ}, p_{T}^{μ}) space. For the J/ψ analysis this separation is defined by the contour that roughly matches a global muon reconstruction efficiency of 10%, indicated by the white lines superimposed in Fig. 2, which are described by the conditions

$$\begin{aligned} p_{\mathrm{T}}^{\mu} &> 3.4\,\mathrm{GeV}/c && \text{for } |\eta^{\mu}| < 1.0, \\ p_{\mathrm{T}}^{\mu} &> (5.8 - 2.4 \times |\eta^{\mu}|)\,\mathrm{GeV}/c && \text{for } 1.0 < |\eta^{\mu}| < 1.5, \\ p_{\mathrm{T}}^{\mu} &> (3.4 - 0.78 \times |\eta^{\mu}|)\,\mathrm{GeV}/c && \text{for } 1.5 < |\eta^{\mu}| < 2.4. \end{aligned} \tag{1}$$

Muons failing these conditions are accounted for in the acceptance corrections discussed in Section 5.1. Muons that pass this acceptance requirement can still fail to pass the trigger, track reconstruction, or muon selection requirements. These losses are accounted for by the efficiency corrections discussed in Section 5.2.

For the $\Upsilon(1S)$ analysis, where the signal-to-background ratio is less favourable than in the J/ψ mass range, a higher p_{T}^{μ} is required than for the J/ψ analysis,

$$p_{\mathrm{T}}^{\mu} > 4\,\mathrm{GeV}/c, \tag{2}$$

independent of η^{μ}.

Various additional global muon selection criteria are studied in MC simulations. The MC distributions of the J/ψ decay muons are in agreement with those from data to better than 2%, which is within the systematic uncertainty of the data/MC efficiency ratio (Section 5.2). The transverse (longitudinal) distance of closest approach to the measured vertex is required to be less than 3 (15) cm. Tracks are only kept if they have 11 or more hits in the silicon tracker, and the χ^2 per degree of freedom of the global (inner) track fit is less than 20 (4). The χ^2 probability of the two tracks originating from a common vertex is required to be larger than 1%. From MC

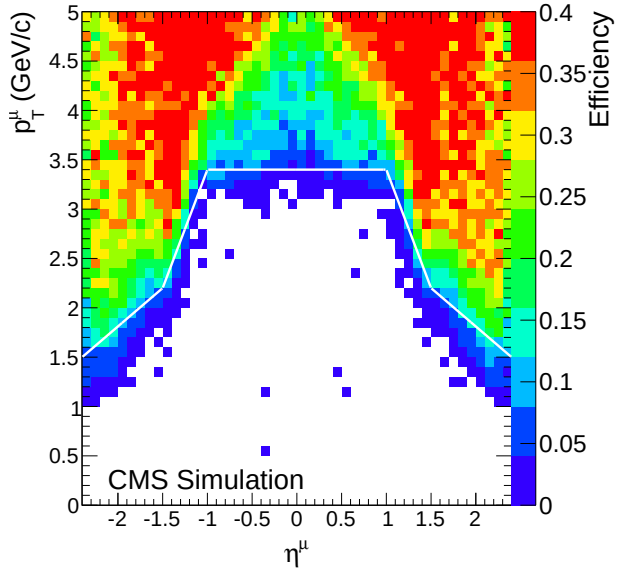

Figure 2: Reconstruction efficiency of global muons in the (η^μ, p_T^μ) space, illustrating the lower limits (white lines) of what is considered a detectable single muon for the J/ψ analysis.

simulations we find that these criteria result in a 6.6%, 5.1%, and 3.9% loss of prompt J/ψ, non-prompt J/ψ, and Υ(1S) events, respectively, given two reconstructed tracks associated with the double muon trigger.

4 Signal Extraction

4.1 J/ψ Analysis

4.1.1 Inclusive J/ψ

The $\mu^+\mu^-$ pair invariant-mass $m_{\mu\mu}$ spectrum is shown in Fig. 3 in the region $2 < m_{\mu\mu} < 4\,\text{GeV}/c^2$ for muon pairs with $0 < p_T < 30\,\text{GeV}/c$ and rapidity $|y| < 2.4$, after applying the single-muon quality requirements. No minimum pair-p_T requirement is applied explicitly. However, the CMS acceptance for $\mu^+\mu^-$ pairs in this mass range requires a minimum p_T that is strongly y-dependent and is $\approx 6.5\,\text{GeV}/c$ at $y = 0$. The black curve in Fig. 3 represents an unbinned maximum likelihood fit to the $\mu^+\mu^-$ pair spectrum, with the signal described by the sum of a Gaussian and a Crystal Ball function, with common mean m_0 and width σ, and the background described by an exponential. The Crystal Ball function $f_{CB}(m)$ combines a Gaussian core and a power-law tail with an exponent n to account for energy loss due to final-state photon radiation,

$$f_{CB}(m) = \begin{cases} \frac{N}{\sqrt{2\pi}\sigma} \exp\left(-\frac{(m-m_0)^2}{2\sigma^2}\right), & \text{for } \frac{m-m_0}{\sigma} > -\alpha; \\ \frac{N}{\sqrt{2\pi}\sigma} \left(\frac{n}{|\alpha|}\right)^n \exp\left(-\frac{|\alpha|^2}{2}\right) \left(\frac{n}{|\alpha|} - |\alpha| - \frac{m-m_0}{\sigma}\right)^{-n}, & \text{for } \frac{m-m_0}{\sigma} \leq -\alpha. \end{cases} \quad (3)$$

The parameter α defines the transition between the Gaussian and the power-law functions. The fit function has eight free parameters; in addition to the five parameters used in Eq. (3), one parameter is the fraction of the Gaussian contribution to the total signal yield (typically ≈ 0.47) and two parameters define the normalization and the slope of the exponential background. The fitted mean value, $m_0 = (3.090 \pm 0.002)\,\text{GeV}/c^2$, is 0.2% below the PDG value of $m_{J/\psi} = 3.097\,\text{GeV}/c^2$ [49] because of slight momentum scale biases in the data reconstruction; the width

is $\sigma = (39 \pm 2)\,\mathrm{MeV}/c^2$, consistent with MC expectations. The number of inclusive J/ψ mesons obtained by the fit is 734 ± 54.

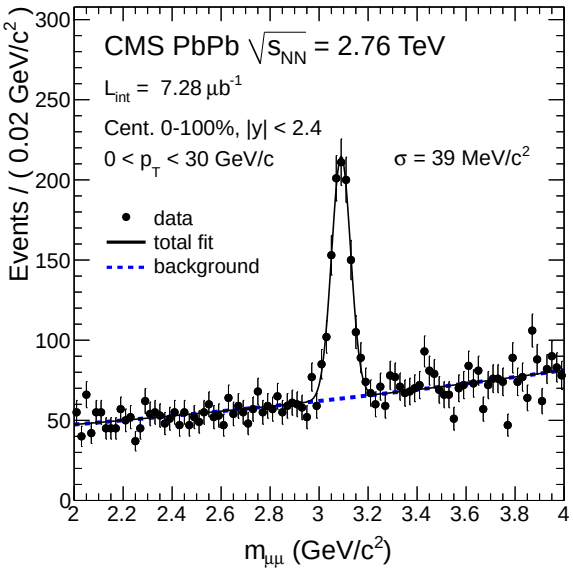

Figure 3: Invariant-mass spectrum of $\mu^+\mu^-$ pairs (black circles) with $|y| < 2.4$ and $0 < p_\mathrm{T} < 30\,\mathrm{GeV}/c$ integrated over centrality. The fit to the data with the functions discussed in the text is shown as the black line. The dashed blue line shows the fitted background contribution.

The analysis is performed in bins of the J/ψ meson p_T and y, as well as in bins of event centrality. Integrating over all centrality (0–100%) and p_T ($6.5 < p_\mathrm{T} < 30\,\mathrm{GeV}/c$) the rapidity bins are

$$|y| < 1.2,\ 1.2 < |y| < 1.6,\ \text{and}\ 1.6 < |y| < 2.4.$$

For the two forward bins, the CMS acceptance extends to lower p_T, so results are also presented for the bins

$$1.2 < |y| < 1.6 \text{ and } 5.5 < p_\mathrm{T} < 30\,\mathrm{GeV}/c,\ \text{as well as } 1.6 < |y| < 2.4 \text{ and } 3 < p_\mathrm{T} < 30\,\mathrm{GeV}/c.$$

These values allow a better comparison with the low-p_T measurements of the ALICE experiment, which has acceptance for J/ψ with $p_\mathrm{T} > 0\,\mathrm{GeV}/c$ for the rapidity intervals $|y| < 0.9$ and $2.4 < y < 4.0$, in the electron and muon decay channels, respectively [50].

Integrating over all centrality (0–100%) and rapidity ($|y| < 2.4$) the p_T bins are

$$6.5 < p_\mathrm{T} < 10\,\mathrm{GeV}/c \text{ and } 10 < p_\mathrm{T} < 30\,\mathrm{GeV}/c.$$

Integrating over the p_T range $6.5 < p_\mathrm{T} < 30\,\mathrm{GeV}/c$ and rapidity $|y| < 2.4$, the centrality bins are: 0–10%, 10–20%, 20–30%, 30–40%, 40–50%, and 50–100%.

The unbinned maximum likelihood fit with the sum of Crystal Ball and Gaussian functions is performed in each of these bins. Because of the small sample size, the parameters of the signal shape are determined for each rapidity and p_T interval, integrated over centrality, as the dominant effect on the mass shape is the p_T- and rapidity-dependent mass resolution. As a function of rapidity, the width of the Crystal Ball function varies from $24\,\mathrm{MeV}/c^2$ ($|y| < 1.2$) to $51\,\mathrm{MeV}/c^2$ ($1.6 < |y| < 2.4$), for the p_T range $6.5 < p_\mathrm{T} < 30\,\mathrm{GeV}/c$. As a function of p_T, the

width changes from 39 MeV/c^2 ($6.5 < p_{\mathrm{T}} < 10$ GeV/c) to 23 MeV/c^2 ($10 < p_{\mathrm{T}} < 30$ GeV/c), when integrated over rapidity. The values are then fixed for the finer centrality bins. The background shape is allowed to vary in each bin. The raw yields of inclusive J/ψ are listed in Table 4 of Appendix A.

4.1.2 Prompt and Non-prompt J/ψ

The identification of J/ψ mesons coming from b-hadron decays relies on the measurement of a secondary $\mu^+\mu^-$ vertex displaced from the primary collision vertex. The displacement vector between the $\mu^+\mu^-$ vertex and the primary vertex $\vec{r}$ is measured in the plane transverse to the beam direction. The most probable transverse b-hadron decay length in the laboratory frame [51, 52] is calculated as

$$L_{xy} = \frac{\hat{u}^T S^{-1} \vec{r}}{\hat{u}^T S^{-1} \hat{u}}\,, \tag{4}$$

where $\hat{u}$ is the unit vector in the direction of the J/ψ meson $\vec{p_{\mathrm{T}}}$ and S^{-1} is the inverse of the sum of the primary and secondary vertex covariance matrices. From L_{xy} the pseudo-proper decay length $\ell_{\mathrm{J}/\psi} = L_{xy}\, m_{\mathrm{J}/\psi} / p_{\mathrm{T}}$ is computed as an estimate of the b-hadron decay length. The pseudo-proper decay length is measured with a resolution of $\sim$35 μm.

To measure the fraction of non-prompt J/ψ, the invariant-mass spectrum of $\mu^+\mu^-$ pairs and their $\ell_{\mathrm{J}/\psi}$ distribution are fitted simultaneously using a two-dimensional unbinned maximum-likelihood fit in bins of p_{T}, rapidity, and centrality with the fraction of non-prompt J/ψ as a free parameter. The fitting procedure is similar to the one used in the pp analysis at $\sqrt{s}$ = 7 TeV [27]. The differences are: (i) the parametrisation of the $\ell_{\mathrm{J}/\psi}$ resolution function and (ii) the MC template used for the true $\ell_{\mathrm{J}/\psi}$ distribution of generated non-prompt J/ψ for which both muons have been reconstructed. Regarding (i), the reconstructed $\ell_{\mathrm{J}/\psi}$ distribution of simulated prompt J/ψ is better parametrised with a resolution function that is the sum of four Gaussians (the pp analysis at 7 TeV used the sum of three Gaussians). Four of the eight fit parameters are fixed to the MC fit result and only the common mean, two widths, and one relative fraction are left free in the fits to the data. Regarding (ii), the $\ell_{\mathrm{J}/\psi}$ distribution of non-prompt J/ψ differs from that of the pp analysis because of the different heavy-ion tracking algorithm. In order to cope with the much higher detector occupancy, the PbPb tracking algorithm is done in one iteration and requires a pixel triplet seed to point to the reconstructed primary vertex within 1 mm. Furthermore, the algorithm includes a filter at the last step that requires the track to point back to the primary vertex within six times the primary vertex resolution. This reduces the reconstruction efficiency for J/ψ with large values of $\ell_{\mathrm{J}/\psi}$, i.e. it causes a difference in the prompt and non-prompt J/ψ reconstruction efficiencies that increases with the J/ψ meson p_{T}.

The prompt J/ψ result is presented (in Section 7.1) in the centrality bins 0–10%, 10–20%, 20–30%, 30–40%, 40–50%, and 50–100%, while the non-prompt J/ψ result, given the smaller sample, is presented (in Section 7.2) in only two centrality bins, 0–20% and 20–100%. Examples of $m_{\mu^+\mu^-}$ and $\ell_{\mathrm{J}/\psi}$ distributions are shown in Fig. 4, including the one for the 0–10% centrality bin, which is one of the worst in terms of signal over background ratio. The two-dimensional fit results are shown as projections onto the mass and $\ell_{\mathrm{J}/\psi}$ axes. Integrated over centrality, the numbers of prompt and non-prompt J/ψ mesons with $|y| < 2.4$ and $6.5 < p_{\mathrm{T}} < 30$ GeV/c are 307 ± 22 and 90 ± 13, respectively.

In order to determine the systematic uncertainty on the yield extraction, the signal and background shapes are varied: for the signal mass shape, in addition to the default sum of the Crystal Ball and Gaussian functions, a single Gaussian and a single Crystal Ball function are tried. Alternatively, the α and n parameters of the Crystal Ball function are fixed individu-

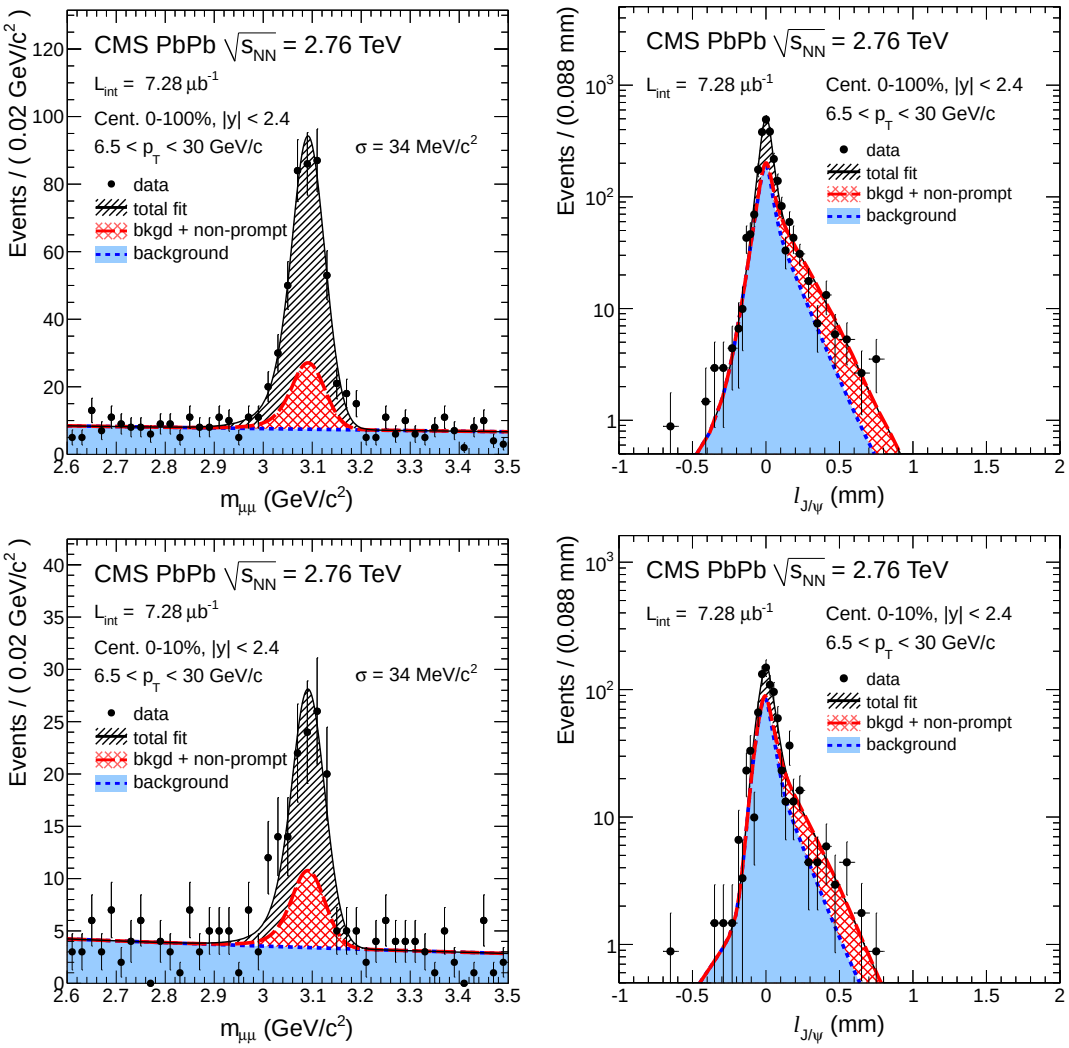

Figure 4: Invariant-mass spectra (left) and pseudo-proper decay length distributions (right) of $\mu^+\mu^-$ pairs integrated over centrality (top) and for the 0–10% centrality bin (bottom). The spectra are integrated over the rapidity range $|y| < 2.4$ and the p_T range $6.5 < p_T < 30\,\mathrm{GeV}/c$. The projections of the two-dimensional fit onto the respective axes are overlaid as solid black lines. The dashed red lines show the fitted contribution of non-prompt J/ψ. The fitted background contributions are shown as dotted blue lines.

ally for each p_T and rapidity bin to the values found in the centrality integrated bin. This is in contrast to the default procedure in which the values for each rapidity bin are fixed to the values found in the bin integrated over centrality and all p_T. For the background mass shape, a straight line is tried as an alternative. A crosscheck using a simple counting of the yield in the signal region after the subtraction of the same-sign spectrum leads to consistent results. The uncertainty on the fraction of non-prompt J/ψ due to the parametrisation of the $\ell_{J/\psi}$ distribution is estimated by varying the number of free parameters in the resolution function while the other parameters are fixed to their MC values. The systematic uncertainty is taken as the RMS of the yields obtained from the different variations of the fit function. The systematic uncertainties vary between 0.5% and 5.7% for the prompt J/ψ yield, while the non-prompt J/ψ yield has uncertainties up to the extreme case of 14% in the most forward rapidity ($1.6 < |y| < 2.4$) and lowest p_T ($3 < p_T < 30\,\text{GeV}/c$) bin.

4.2 $\Upsilon(1S)$ Analysis

To extract the $\Upsilon(1S)$ yield, an extended unbinned maximum-likelihood fit to the $\mu^+\mu^-$ invariant mass spectrum between 7 and $14\,\text{GeV}/c^2$ is performed, integrated over p_T, rapidity, and centrality, as shown in the left panel of Fig. 5. The measured mass line shape of each Y state is parametrised by a Crystal Ball function. Since the three Y resonances partially overlap in the measured dimuon mass spectrum, they are fitted simultaneously. Therefore, the probability distribution function describing the signal consists of three Crystal Ball functions. In addition to the three Y(nS) yields, the $\Upsilon(1S)$ mass is the only parameter left free, to accommodate a possible bias in the momentum scale calibration. The mass ratios between the states are fixed to their world average values [49], and the mass resolution is forced to scale linearly with the resonance mass. The $\Upsilon(1S)$ resolution is fixed to the value found in the simulation, $92\,\text{MeV}/c^2$. This value is consistent with what is measured when leaving this parameter free in a fit to the data, $(122 \pm 30)\,\text{MeV}/c^2$. The low-side tail parameters in the Crystal Ball function are also fixed to the values obtained from simulation. Finally, a second-order polynomial is chosen to describe the background in the mass range 7–$14\,\text{GeV}/c^2$. From this fit, before accounting for acceptance and efficiencies, the measured $\Upsilon(1S)$ raw yield is 86 ± 12. The observed suppression of the excited states was discussed in [25]. The fitted mean value is $m_0 = (9.441 \pm 0.016)\,\text{GeV}/c^2$, which, for the same reason as for the J/ψ, is slightly below the PDG value $m_{\Upsilon(1S)} = 9.460\,\text{GeV}/c^2$ [49].

The data are binned in p_T and rapidity of the $\mu^+\mu^-$ pairs, as well as in bins of the event centrality (0–10%, 10–20%, and 20–100%). The bins in rapidity are $|y| < 1.2$ and $1.2 < |y| < 2.4$. In contrast to the J/ψ case, CMS has acceptance for Y down to $p_T = 0\,\text{GeV}/c$ over the full rapidity range. The p_T bins in this analysis are $0 < p_T < 6.5\,\text{GeV}/c$, $6.5 < p_T < 10\,\text{GeV}/c$, and $10 < p_T < 20\,\text{GeV}/c$. There are only two events with a $\mu^+\mu^-$ pair in the Y mass region and $p_T > 20\,\text{GeV}/c$. The invariant-mass distribution for the centrality bin 0–10% is illustrated in the right panel of Fig. 5. The raw yields of $\Upsilon(1S)$are tabulated in Table 5 of Appendix A.

The systematic uncertainties are computed by varying the line shape in the following ways: (i) the Crystal Ball function tail parameters are varied randomly according to their covariance matrix and within conservative values covering imperfect knowledge of the amount of detector material and final-state radiation in the underlying process; (ii) the width is varied by $\pm 5\,\text{MeV}/c^2$, a value motivated by the current understanding of the detector performance (e.g., the dimuon mass resolution, accurately measured at the J/ψ mass, is identical in pp and PbPb collisions); (iii) the background shape is changed from quadratic to linear, and the mass range of the fit is varied from 6–15 to 8–$12\,\text{GeV}/c^2$; the observed RMS of the results in each category is taken as the systematic uncertainty. The quadratic sum of these three systematic uncertainties is dominated by the variation of the resolution of the mass fit, and is of the order of 10%, reach-

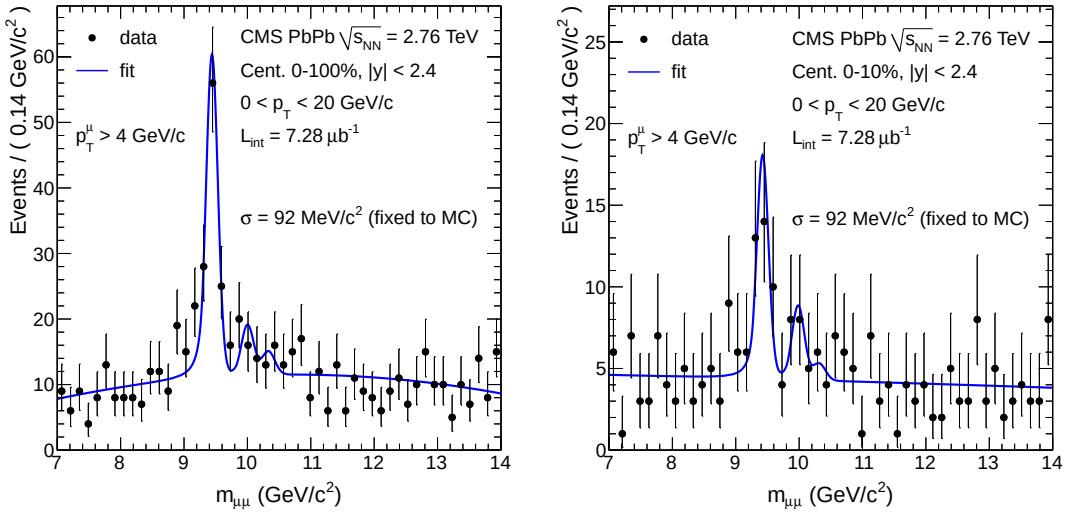

Figure 5: Invariant-mass spectrum of $\mu^+\mu^-$ pairs (black circles) with $p_T < 20\,\text{GeV}/c$ and $|y| < 2.4$, for muons above $4\,\text{GeV}/c$, integrated over centrality (left) and for the 0–10% centrality bin (right).

ing 13% for the 0–10% centrality bin. As was the case for the J/ψ selection, a simple counting of the yield in the signal region after the subtraction of the same-sign spectrum leads to consistent results.

5 Acceptance and Efficiency

5.1 Acceptance

The dimuon acceptance, A, is defined as the fraction of $\mu^+\mu^-$ pairs for which both muons are declared detectable in the CMS detector with respect to all muon pairs produced in $|y| < 2.4$,

$$A(p_T, y; \lambda_\theta) = \frac{N^{\mu\mu}_{\text{detectable}}(p_T, y; \lambda_\theta)}{N^{\mu\mu}_{\text{generated}}(p_T, y; \lambda_\theta)}, \tag{5}$$

where:

- $N^{\mu\mu}_{\text{detectable}}$ is the number of generated events in a given quarkonium (p_T, y) bin in the MC simulation, for which both muons are detectable according to the selections defined in Eqs. (1) and (2);
- $N^{\mu\mu}_{\text{generated}}$ is the number of all $\mu^+\mu^-$ pairs generated within the considered (p_T, y) bin.

The acceptance depends on the p_T and y of the $\mu^+\mu^-$ pair, and the polarization parameter λ_θ. Different polarizations of the J/ψ and Υ(1S) will cause different single-muon angular distributions in the laboratory frame and, hence, different probabilities for the muons to fall inside the CMS detector acceptance. Since the quarkonium polarization has not been measured in heavy-ion or pp collisions at $\sqrt{s_{NN}} = 2.76\,\text{TeV}$, the prompt J/$\psi$ and Υ(1S) results are quoted for the unpolarized scenario only. For non-prompt J/ψ the results are reported for the polarization predicted by EVTGEN. The impact of the polarization on the acceptance is studied for the most extreme polarization scenarios in the Collins–Soper and helicity frames. For fully longitudinal (transverse) polarized J/ψ in the Collins–Soper frame, the effect is found to be at most

−20% (6%). In the helicity frame, the effects are at most 40% and −20% for the two scenarios. For Υ(1S) the polarization effects range between −20% for longitudinal polarization in the Collins–Soper frame to 40% for transverse polarization in the helicity frame.

The acceptance is calculated using the MC sample described in Section 3.1. The p_T and rapidity dependencies of the J/ψ and Υ(1S) acceptances are shown in Fig. 6.

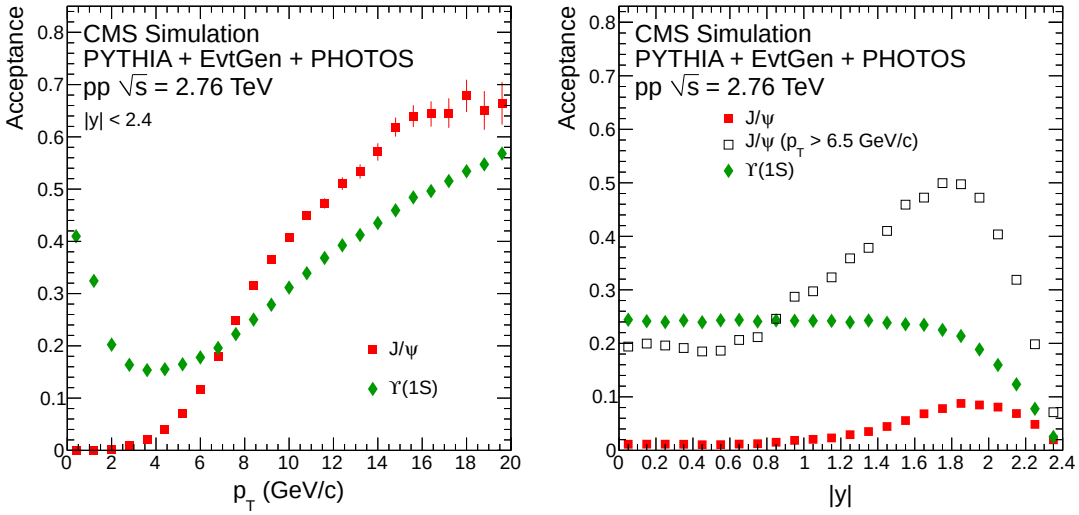

Figure 6: Dimuon acceptance as a function of p_T (left) and $|y|$ (right) for J/ψ (red squares) and Υ(1S) (green diamonds). Also shown in the right panel is the acceptance for J/ψ with $p_T > 6.5\,\text{GeV}/c$ (open black squares). The error bars represent the statistical uncertainties only.

Since the acceptance is a function of both p_T and y, uncertainties in the predicted distributions for these variables can lead to a systematic uncertainty in the average acceptance over a p_T or y bin. To estimate these uncertainties, the shapes of the generated MC p_T and $|y|$ distributions are varied by applying a weight that increases linearly from 0.7 to 1.3 over the range $0 < |y| < 2.4$ and $0 < p_T < 30\,\text{GeV}/c$ ($20\,\text{GeV}/c$) for J/ψ (Υ(1S)). The RMS of the resulting changes in the acceptance for each p_T and y bin are summed in quadrature to compute the overall systematic uncertainty from this source. The largest relative systematic uncertainties obtained are 4.2%, 3.2%, and 2.8% for the prompt J/ψ, non-prompt J/ψ, and Υ(1S) acceptances, respectively.

5.2 Efficiency

The trigger, reconstruction, and selection efficiencies of $\mu^+\mu^-$ pairs are evaluated using simulated MC signal events embedded in simulated PbPb events, as described in Section 3.1. The overall efficiency is calculated, in each analysis bin, as the fraction of generated events (passing the single muon phase space cuts) where both muons are reconstructed, fulfil the quality selection criteria and pass the trigger requirements. In the embedded sample, the signal over background ratio is by construction higher than in data, so the background contribution underneath the resonance peak is negligible and the signal is extracted by simply counting the $\mu^+\mu^-$ pairs in the quarkonium mass region. The counting method is crosschecked by using exactly the same fitting procedure as if the MC events were collision data. Only muons in the kinematic region defined by Eqs. (1) and (2) are considered.

In Fig. 7, the efficiencies are shown as a function of the $\mu^+\mu^-$ pair p_T, y, and the event centrality, for each signal: red squares for prompt J/ψ, orange stars for non-prompt J/ψ, and green diamonds for Υ(1S). As discussed in Section 4.1.2, the efficiency of non-prompt J/ψ is lower than that of prompt J/ψ, reaching about 35% for $p_T > 12\,\text{GeV}/c$. The prompt J/ψ efficiency

increases with p_T until reaching a plateau slightly above 50% at p_T of about 12 GeV/c, while the Υ(1S) efficiency is $\sim$55%, independent of p_T. The efficiencies decrease slowly as a function of centrality because of the increasing occupancy in the silicon tracker; the relative difference between peripheral and central collisions is 17% for J/ψ and 10% for Υ(1S). The integrated efficiency values are 38.3%, 29.2%, and 54.5% for the prompt J/ψ, non-prompt J/ψ (both with $6.5 < p_T < 30$ GeV/c, $|y| < 2.4$, and 0–100% centrality), and Υ(1S) (with $0 < p_T < 20$ GeV/c, $|y| < 2.4$, and 0–100% centrality), respectively.

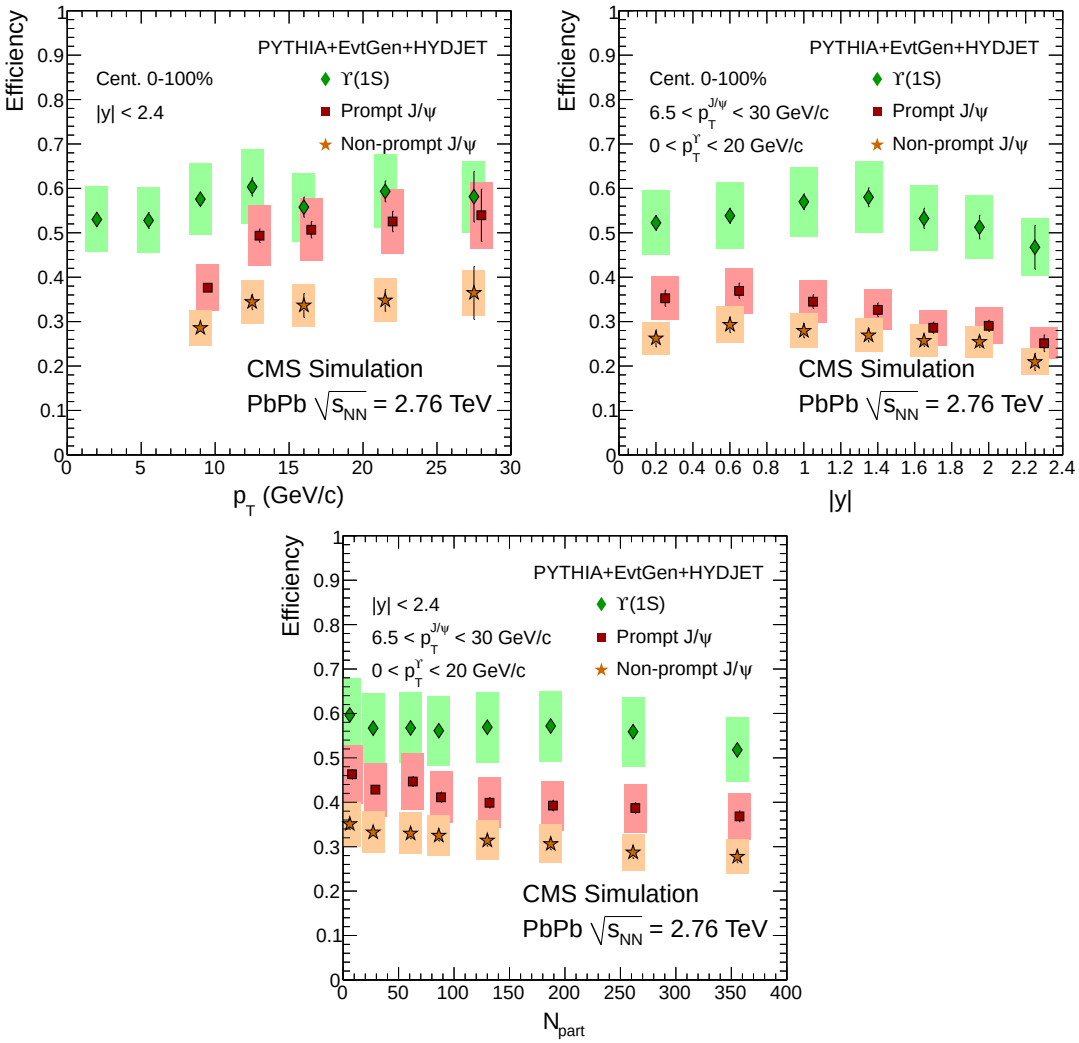

Figure 7: Combined trigger, reconstruction, and selection efficiencies as a function of quarkonium p_T and $|y|$, and event centrality, for each signal: red squares and orange stars for prompt and non-prompt J/ψ, respectively, and green diamonds for Υ(1S). For better visibility, the prompt J/ψ points are shifted by $\Delta p_T = 0.5$ GeV/c, $\Delta y = 0.05$, and $\Delta N_{part} = 2$. Statistical (systematic) uncertainties are shown as bars (boxes). The systematic uncertainties are the quadratic sum of the uncertainty on the kinematic distributions and the MC validation uncertainty.

The systematic uncertainty on the final corrections due to the kinematic distributions is estimated by a $\pm$30% variation of the slopes of the generated p_T and rapidity shapes, similar to the acceptance variation described in the previous section. The systematic uncertainties are in the ranges 1.8–3.4%, 2.2–4.2%, and 1.4–2.7% for prompt J/ψ, non-prompt J/ψ, and Υ(1S), respectively, including the statistical precision of the MC samples.

The individual components of the MC efficiency are crosschecked using muons from J/ψ decays in simulated and collision data with a technique called *tag-and-probe*, similar to the one used for the corresponding pp measurement [27]. In this method, high quality muons (the *tags*) are combined with muons that are selected without applying the selections whose efficiency is to be measured (the *probes*). Probe muons that fulfil these selections are then categorized as *passing probes*, the others as *failing probes*. A simultaneous fit of the two resulting invariant mass spectra (passing and failing) provides the efficiency of the probed selection. Because of correlations in the efficiency of matching silicon-tracker tracks to standalone muons, the total efficiency does not fully factorize into the individual components probed by this method. Therefore, the reconstruction and trigger efficiencies for $\mu^+\mu^-$ pairs are directly obtained from the MC simulation, rather than as a product of the partial components.

The fits are performed for *tag-probe* pairs with a p_{T} above 6.5 GeV/c as this is the region measured over the full rapidity range, with and without applying the probed selection on one of the muons:

1. The trigger efficiency is estimated by measuring the fraction of global muons (used as probes) associated to the double-muon trigger in an event sample selected by tag-muons associated to a single-muon trigger. A Crystal Ball function is used to describe the J/ψ peak. The p_{T}^{μ} and η^{μ} dependencies of the trigger efficiency are compatible between data and MC. For J/ψ with $p_{\mathrm{T}} > 6.5\,\mathrm{GeV}/c$, the p_{T}^{μ} and η^{μ} integrated trigger efficiency is 95.9% in MC and (95.1 ± 0.9)% in data.

2. Standalone muons passing the quality selections required in this analysis are used to evaluate the efficiency of the silicon tracker reconstruction, which includes losses induced by the matching between the silicon-tracker track and the muon detector track, and by the imposed quality selection criteria (both on the global track and on its silicon-tracker segment). For this efficiency measurement, the signal is fitted with a Gaussian function and the background with a second-order polynomial. A Gaussian, rather than a Crystal Ball function, is used because of the poor momentum resolution of the standalone muons. No $p_{\mathrm{T}} > 6.5\,\mathrm{GeV}/c$ requirement was used, since the poorer momentum resolution of standalone muons would have biased the measurement. The single-muon efficiencies measured in MC and data of 84.9% and $(83.7^{+5.7}_{-5.3})$%, respectively, are in good agreement.

The systematic uncertainty of the muon pair efficiency, 13.7%, is determined by comparing the *tag-and-probe* efficiencies evaluated in PbPb data and MC samples, and is dominated by the statistical uncertainties of the measurements. The standalone muon reconstruction efficiency (99% in the plateau) cannot be probed with silicon-tracker tracks because of the large charged particle multiplicity in PbPb collisions. Since this part of the reconstruction is identical to that used for pp data, a systematic uncertainty of 1%, reported in Ref. [53], is assumed.

6 The pp Baseline Measurement

A pp run at $\sqrt{s} = 2.76\,\mathrm{TeV}$ was taken in March 2011. The integrated luminosity was $231\,\mathrm{nb}^{-1}$, with an associated uncertainty of 6%. For hard-scattering processes, the integrated luminosity of the pp sample is comparable to that of the PbPb sample ($7.28\,\mu\mathrm{b}^{-1} \cdot 208^2 \approx 315\,\mathrm{nb}^{-1}$).

Given the higher instantaneous luminosity, the Level-1 trigger required slightly higher quality muons in the pp run than in the PbPb run. The offline event selection is the same as in the PbPb analysis, only slightly relaxed for the HF coincidence requirement: instead of three towers, only

one tower with at least 3 GeV deposited is required in the pp case. The same reconstruction algorithm, i.e. the one optimized for the heavy-ion environment, is used for both pp and PbPb data. The products of the trigger, reconstruction, and selection efficiencies determined in pp MC simulations are 42.5%, 34.5%, and 55.1% for the prompt J/ψ, non-prompt J/ψ (both with $6.5 < p_{\mathrm{T}} < 30\,\mathrm{GeV}/c$, $|y| < 2.4$), and $\Upsilon(1S)$ (with $0 < p_{\mathrm{T}} < 20\,\mathrm{GeV}/c$, $|y| < 2.4$), respectively.

The accuracy of the MC simulation in describing the trigger efficiency is crosschecked with the *tag-and-probe* method in the same way as for the PbPb analysis discussed in Section 5.2. For muons from decays of J/ψ with $p_{\mathrm{T}} > 6.5\,\mathrm{GeV}/c$, the p_{T}^{μ} and η^{μ} integrated trigger efficiencies are $(92.5 \pm 0.6)\%$ in data and $(94.3 \pm 0.2)\%$ in MC. In the same phase-space, the tracking and muon selection efficiency is $(82.5 \pm 2.4)\%$ in data and $(84.6 \pm 1.0)\%$ in MC. For the standalone muon reconstruction efficiency a systematic uncertainty of 1% is assigned, as reported in Ref. [53]. As in the PbPb case, the systematic uncertainty of the muon pair efficiency in pp collisions, 13.7%, is determined by comparing the *tag-and-probe* efficiencies evaluated in data and MC samples, and is dominated by the statistical uncertainties of the measurements.

The quarkonium signals in pp collisions are extracted following the same methods as in PbPb collisions, described in Sections 4.1 and 4.2, apart from the non-prompt J/ψ signal extraction: the four Gaussians of the lifetime resolution are fixed to the MC values because of the lack of events in the dimuon mass sidebands. The systematic uncertainty on the signal extraction in pp is 10% for $\Upsilon(1S)$ and varies, depending on p_{T} and rapidity, between 0.4 and 6.2% for prompt J/ψ and between 5 and 20% for non-prompt J/ψ. The fit results for the prompt and non-prompt J/ψ yield extraction are shown in Fig. 8 for $|y| < 2.4$ and $6.5 < p_{\mathrm{T}} < 30\,\mathrm{GeV}/c$. The numbers of prompt and non-prompt J/ψ mesons in this rapidity and p_{T} range are 820 ± 34 and 206 ± 20, respectively.

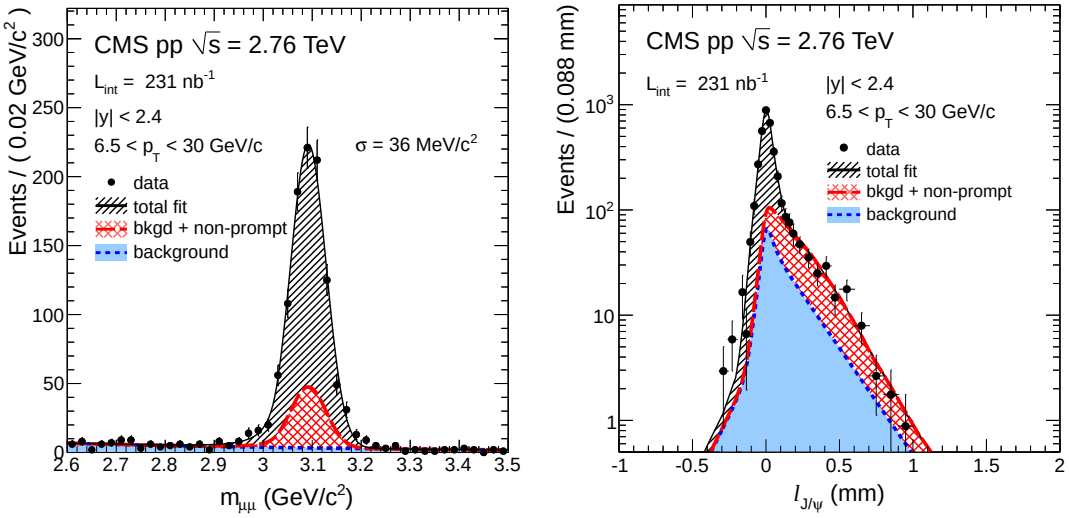

Figure 8: Non-prompt J/ψ signal extraction for pp collisions at $\sqrt{s} = 2.76\,\mathrm{TeV}$: dimuon invariant mass fit (left) and pseudo-proper decay length fit (right).

The invariant-mass spectrum of $\mu^+\mu^-$ pairs in the Υ region from pp collisions is shown in Fig. 9. The same procedure as the one described for the PbPb analysis is used. The number of $\Upsilon(1S)$ mesons with $|y| < 2.4$ and $0 < p_{\mathrm{T}} < 20\,\mathrm{GeV}/c$ is 101 ± 12. The fit result of the excited states is discussed in [25].

The differential cross section results include the systematic uncertainties of the reconstruction efficiency and acceptance, estimated in the same way as for the PbPb analysis. The systematic

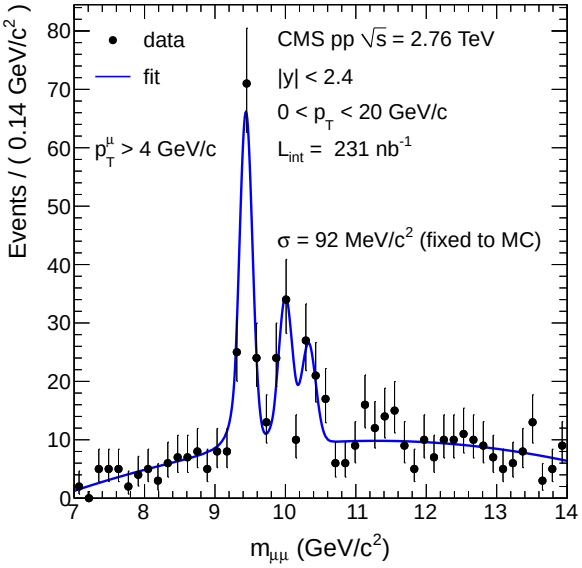

Figure 9: The pp dimuon invariant-mass distribution in the range $p_T < 20\,\text{GeV}/c$ for $|y| < 2.4$ and the result of the fit to the Y resonances.

uncertainties on the efficiencies are 1.6–3%, 1.4–2%, and 0.4–0.9% for prompt J/ψ, non-prompt J/ψ, and Υ(1S), respectively. The uncertainty on the acceptance is identical in the pp and PbPb analyses.

For the measurement of the nuclear modification factors, in which the ratio of PbPb to pp results is computed, most of the reconstruction systematic uncertainties cancel out because the same algorithm is used. However, the following factors must be accounted for:

1. The luminosity uncertainty. This is a global systematic uncertainty of 6% that allows all measured nuclear modification factors to change by a common scale-factor. Since the PbPb yield is normalized by the number of minimum-bias events, which has a negligible uncertainty, no systematic uncertainty on the PbPb luminosity has to be considered.

2. The uncertainty on T_{AA}. For results integrated over centrality, this is a global systematic uncertainty of 5.7%, based on the Glauber model employed. For results as a function of centrality, the uncertainty varies between a minimum of 4.3% in the most central bin and a maximum of 15% in the most peripheral bin [37].

3. The systematic uncertainty associated with the trigger efficiency. The ratios between the *tag-and-probe* efficiencies obtained in pp and PbPb are the same in data and MC events, within the statistical accuracy of the data (1% for the single-muon efficiency). Twice this value (2%) is assigned as the uncertainty on the difference of the trigger efficiencies of $\mu^+\mu^-$ pairs in PbPb and pp collisions.

4. The tracking efficiency uncertainty due to different charged particle multiplicities in pp and PbPb collisions. The ratios between the *tag-and-probe* efficiencies obtained in pp and central PbPb events are the same in data and MC events, within the statistical accuracy of the data (6.8% for the single-muon efficiency). This value is propagated as the tracking systematic uncertainty in all the ratios of PbPb to pp data.

7 Results

The double-differential quarkonium cross sections in PbPb collisions are reported in the form

$$\frac{1}{T_{AA}} \cdot \frac{\mathrm{d}^2 N}{\mathrm{d}y\,\mathrm{d}p_{\mathrm{T}}} = \frac{1}{T_{AA}\,N_{\mathrm{MB}}} \cdot \frac{1}{\Delta y\,\Delta p_{\mathrm{T}}} \cdot \frac{N_{\mathrm{Q\overline{Q}}}}{A\,\varepsilon}, \tag{6}$$

while in pp collisions they are calculated as

$$\frac{d^2\sigma}{\mathrm{d}y\,\mathrm{d}p_{\mathrm{T}}} = \frac{1}{\mathcal{L}_{\mathrm{pp}}} \cdot \frac{1}{\Delta y\,\Delta p_{\mathrm{T}}} \cdot \frac{N_{\mathrm{Q\overline{Q}}}}{A\,\varepsilon}, \tag{7}$$

where:

- $N_{\mathrm{Q\overline{Q}}}$ is the number of measured prompt J/ψ, non-prompt J/ψ, or Υ(1S) in the $\mu^+\mu^-$ decay channel;
- N_{MB} is the number of minimum-bias events sampled by the event selection; when binned in centrality, only the fraction of minimum-bias events in that centrality bin is considered;
- A is the geometric acceptance, which depends on the p_{T} and y of the quarkonium state;
- ε is the combined trigger and reconstruction efficiency, which depends on the p_{T} and y of the quarkonium state and on the centrality of the collision;
- Δy and Δp_{T} are the bin widths in rapidity and p_{T}, respectively;
- T_{AA} is the nuclear overlap function, which depends on the collision centrality;
- $\mathcal{L}_{\mathrm{pp}} = (231 \pm 14)\,\mathrm{nb}^{-1}$ is the integrated luminosity of the pp data set.

Following Eq. (6), the uncorrected yields of inclusive, prompt and non-prompt J/ψ, and Υ(1S), measured in PbPb collisions are corrected for acceptance and efficiency (reported in Figs. 6 and 7), and converted into yields divided by the nuclear overlap function T_{AA}. These quantities can be directly compared to cross sections in pp collisions measured from the raw yields according to Eq. (7). The rapidity and centrality-dependent results are presented integrated over p_{T}. All results are presented for the unpolarized scenario and are tabulated in Tables 6–13 of Appendix A.

The systematic uncertainties detailed in the previous sections are summarized in Tables 2 and 3. The relative uncertainties for all terms appearing in Eqs. (6) and (7) are added in quadrature, leading to a total of 15–21% on the corrected yields. For results plotted as a function of p_{T} or rapidity, the systematic uncertainty on T_{AA} enters as a global uncertainty on the scale and is not included in the systematic uncertainties of the yields. As a function of centrality, the uncertainty on T_{AA} varies point-to-point and is included in the systematic uncertainties of the yields.

The nuclear modification factor,

$$R_{AA} = \frac{\mathcal{L}_{\mathrm{pp}}}{T_{AA} N_{\mathrm{MB}}} \frac{N_{\mathrm{PbPb}}(\mathrm{Q\overline{Q}})}{N_{\mathrm{pp}}(\mathrm{Q\overline{Q}})} \cdot \frac{\varepsilon_{\mathrm{pp}}}{\varepsilon_{\mathrm{PbPb}}}, \tag{8}$$

is calculated from the raw yields $N_{\mathrm{PbPb}}(\mathrm{Q\overline{Q}})$ and $N_{\mathrm{pp}}(\mathrm{Q\overline{Q}})$, correcting only for the multiplicity-dependent fraction of the efficiency ($\frac{\varepsilon_{\mathrm{pp}}}{\varepsilon_{\mathrm{PbPb}}} \sim 1.16$ for the most central bin); the p_{T} and rapidity dependencies of the efficiency cancel in the ratio. These results are also tabulated in Appendix A. It should be noted that the R_{AA} would be sensitive to changes of the J/ψ polarization between pp and PbPb collisions, an interesting physics effect on its own [54].

Table 2: Point-to-point systematic uncertainties on the prompt J/ψ, non-prompt J/ψ, and Υ(1S) yields measured in PbPb collisions.

	prompt J/ψ (%)	non-prompt J/ψ (%)	Υ(1S) (%)
Yield extraction	0.5–5.7	1.5–14.0	8.7–13.4
Efficiency	1.8–3.4	2.2–4.2	1.4–2.7
Acceptance	0.9–4.2	2.0–3.2	1.5–2.8
MC Validation	13.7	13.7	13.7
Stand-alone μ reco.	1.0	1.0	1.0
T_{AA}	4.3–15.0	4.6–8.6	4.3–8.6
Total	15–21	15–21	18–20

Table 3: Point-to-point systematic uncertainties on the prompt J/ψ, non-prompt J/ψ, and Υ(1S) yields measured in pp collisions.

	prompt J/ψ (%)	non-prompt J/ψ (%)	Υ(1S) (%)
Yield extraction	0.8–5.3	5.3–16.8	10.0
Efficiency	1.6–3.0	1.4–2.0	0.4–0.9
Acceptance	0.9–4.2	2.0–3.2	1.5–2.8
MC Validation	13.7	13.7	13.7
Stand-alone μ reco.	1.0	1.0	1.0
Total	14–16	15–22	17–18

In all figures showing results, statistical uncertainties are represented by error bars and systematic uncertainties by boxes. Results as a function of rapidity are averaged over the positive and negative rapidity regions.

7.1 Inclusive and Prompt J/ψ

The inclusive and prompt J/ψ differential yields in PbPb collisions, divided by T_{AA}, are shown in the left panel of Fig. 10 as a function of p_{T}, for $|y| < 2.4$ and integrated over centrality. The corresponding pp cross sections are also shown. The suppression of the prompt J/ψ yield by a factor of ~ 3 with respect to pp is easier to appreciate through the R_{AA} observable, shown in the right panel of Fig. 10. The R_{AA} measurements do not exhibit a p_{T} dependence over the measured p_{T} range, while there is an indication of less suppression in the most forward rapidity bin ($1.6 < |y| < 2.4$) in comparison to the mid-rapidity bin, as shown in Fig. 11. At forward rapidity, in addition to $6.5 < p_{\mathrm{T}} < 30\,\mathrm{GeV}/c$ the nuclear modification factor is measured for lower p_{T} (down to $3\,\mathrm{GeV}/c$) without observing a significant change, as can be seen in Table 7.

The inclusive J/ψ yield in PbPb collisions divided by T_{AA}, integrated over the p_{T} range 6.5–$30\,\mathrm{GeV}/c$ and $|y| < 2.4$, is shown in the left panel of Fig. 12 as a function of N_{part}. Also included is the prompt J/ψ yield, which exhibits the same centrality dependence as the inclusive J/ψ: from the 50–100% centrality bin ($\langle N_{\mathrm{part}} \rangle = 22.1$) to the 10% most central collisions ($\langle N_{\mathrm{part}} \rangle = 355.4$) the yield divided by T_{AA} falls by a factor of ~ 2.6. The results are compared to the cross sections measured in pp, showing that prompt J/ψ are already suppressed in peripheral PbPb collisions. The R_{AA} of prompt J/ψ as a function of N_{part} is shown in the right panel of Fig. 12: a suppression of ~ 5 is observed in the 10% most central PbPb collisions with respect to pp. This suppression is reduced in more peripheral collisions, reaching a factor of ~ 1.6 in the 50–100% centrality bin.

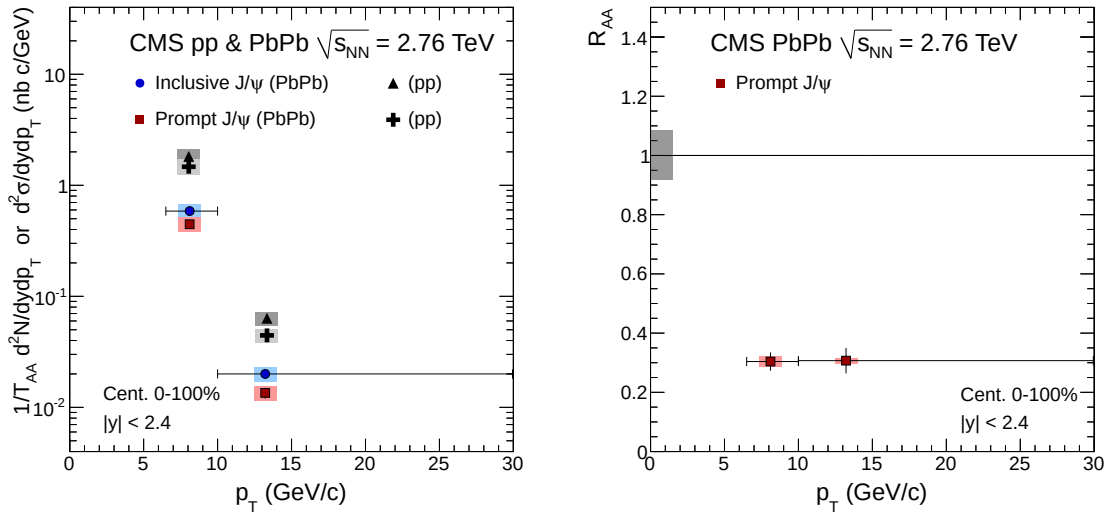

Figure 10: Left: yield of inclusive J/ψ (blue circles) and prompt J/ψ (red squares) divided by T_{AA} as a function of p_{T}. The results are compared to the cross sections of inclusive J/ψ (black triangles) and prompt J/ψ (black crosses) measured in pp. The global scale uncertainties on the PbPb data due to T_{AA} (5.7%) and the pp integrated luminosity (6.0%) are not shown. Right: nuclear modification factor R_{AA} of prompt J/ψ as a function of p_{T}. A global uncertainty of 8.3%, from T_{AA} and the integrated luminosity of the pp data sample, is shown as a grey box at $R_{AA} = 1$. Points are plotted at their measured average p_{T}. Statistical (systematic) uncertainties are shown as bars (boxes). Horizontal bars indicate the bin width.

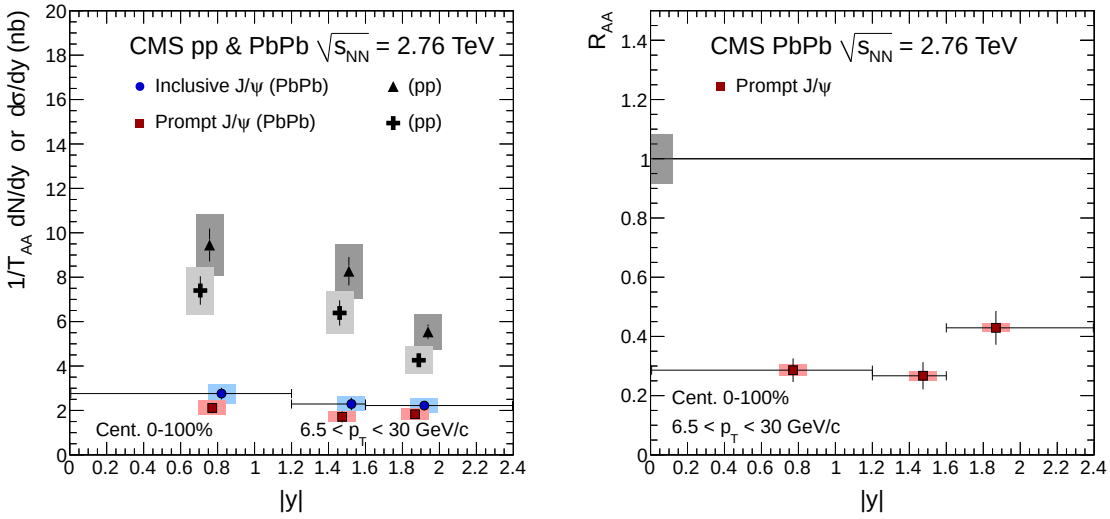

Figure 11: Left: yield of inclusive J/ψ (blue circles) and prompt J/ψ (red squares) divided by T_{AA} as a function of rapidity. The results are compared to the cross sections of inclusive J/ψ (black triangles) and prompt J/ψ (black crosses) measured in pp. The inclusive J/ψ points are shifted by $\Delta y = 0.05$ for better visibility. The global scale uncertainties on the PbPb data due to T_{AA} (5.7%) and the pp luminosity (6.0%) are not shown. Right: nuclear modification factor R_{AA} of prompt J/ψ as a function of rapidity. A global uncertainty of 8.3%, from T_{AA} and the integrated luminosity of the pp data sample, is shown as a grey box at $R_{AA} = 1$. Points are plotted at their measured average $|y|$. Statistical (systematic) uncertainties are shown as bars (boxes). Horizontal bars indicate the bin width.

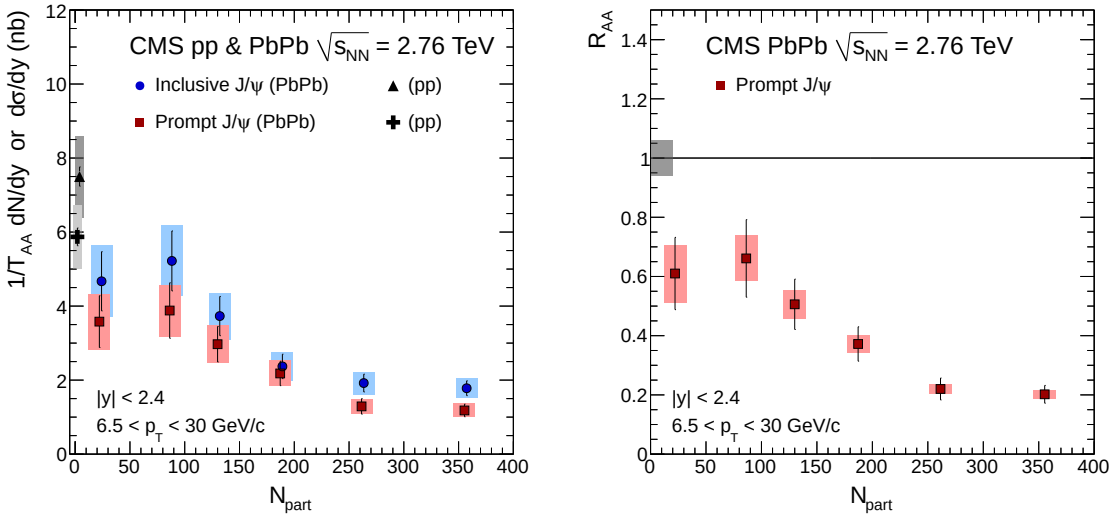

Figure 12: Left: yield of inclusive J/ψ (blue circles) and prompt J/ψ (red squares) divided by T_{AA} as a function of N_{part}. The results are compared to the cross sections of inclusive J/ψ (black triangle) and prompt J/ψ (black cross) measured in pp. The inclusive J/ψ points are shifted by $\Delta N_{\text{part}} = 2$ for better visibility. Right: nuclear modification factor R_{AA} of prompt J/ψ as a function of N_{part}. A global uncertainty of 6%, from the integrated luminosity of the pp data sample, is shown as a grey box at $R_{AA} = 1$. Statistical (systematic) uncertainties are shown as bars (boxes).

7.2 Non-prompt J/ψ

The uncorrected fraction of non-prompt J/ψ is obtained from the two-dimensional fit to the invariant mass and $\ell_{J/\psi}$ spectra discussed in Section 4.1.2. To obtain the corrected b fraction, which is the ratio of non-prompt to inclusive J/ψ, the raw fraction is corrected for the different reconstruction efficiencies and acceptances for prompt and non-prompt J/ψ. The b fraction in pp and in PbPb (integrated over centrality) at $\sqrt{s_{\text{NN}}}$ = 2.76 TeV is presented in Fig. 13 as a function of p_{T}, for several rapidity bins, together with results from CDF [42] and CMS [27] at other collision energies. There is good agreement, within uncertainties, between the earlier results and the present measurements.

The non-prompt J/ψ yield in PbPb collisions divided by T_{AA}, integrated over the p_{T} range 6.5–30 GeV/c and $|y| < 2.4$, is shown in the left panel of Fig. 14 as a function of N_{part}, together with the pp cross section. Non-prompt J/ψ are suppressed by a factor of $\sim$2.6 with respect to pp collisions, as can be seen in the right panel of Fig. 14. The suppression does not exhibit a centrality dependence, but the most peripheral centrality bin (20–100%, $\langle N_{\text{part}} \rangle = 64.2$) is very broad. Hard processes, such as quarkonium and b-hadron production, are produced following a scaling with the number of nucleon-nucleon collisions, thus most events in such a large bin occur towards its most central edge.

7.3 Υ(1S)

In Fig. 15, the Υ(1S) yield divided by T_{AA} in PbPb collisions and its cross section in pp collisions are shown as a function of p_{T}; the R_{AA} of Υ(1S) is displayed in the right panel of Fig. 15. The p_{T} dependence shows a significant suppression, by a factor of $\sim$2.3 at low p_{T}, that disappears for $p_{\text{T}} > 6.5$ GeV/c. The rapidity dependence indicates a slightly smaller suppression at forward rapidity, as shown in Fig. 16. However, the statistical uncertainties are too large to draw strong

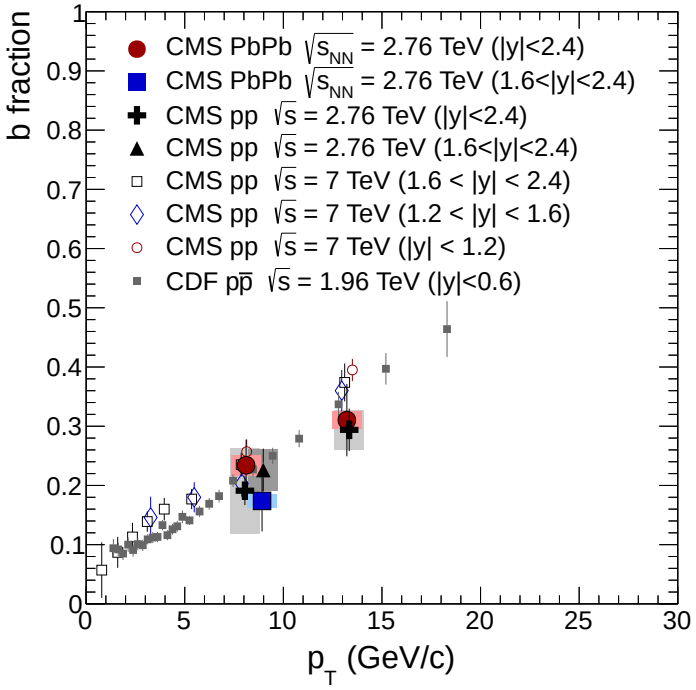

Figure 13: b fraction of J/ψ production in pp and PbPb collisions at $\sqrt{s_{\rm NN}}$ = 2.76 TeV as a function of $p_{\rm T}$ for the rapidity bins $|y| < 2.4$ and $1.6 < |y| < 2.4$, compared to b fractions measured by CDF in p$\overline{\rm p}$ collisions at $\sqrt{s}$ = 1.96 TeV [42] and by CMS in pp collisions at $\sqrt{s}$ = 7 TeV [27]. Points are plotted at their measured average $p_{\rm T}$. Statistical (systematic) uncertainties are shown as bars (boxes).

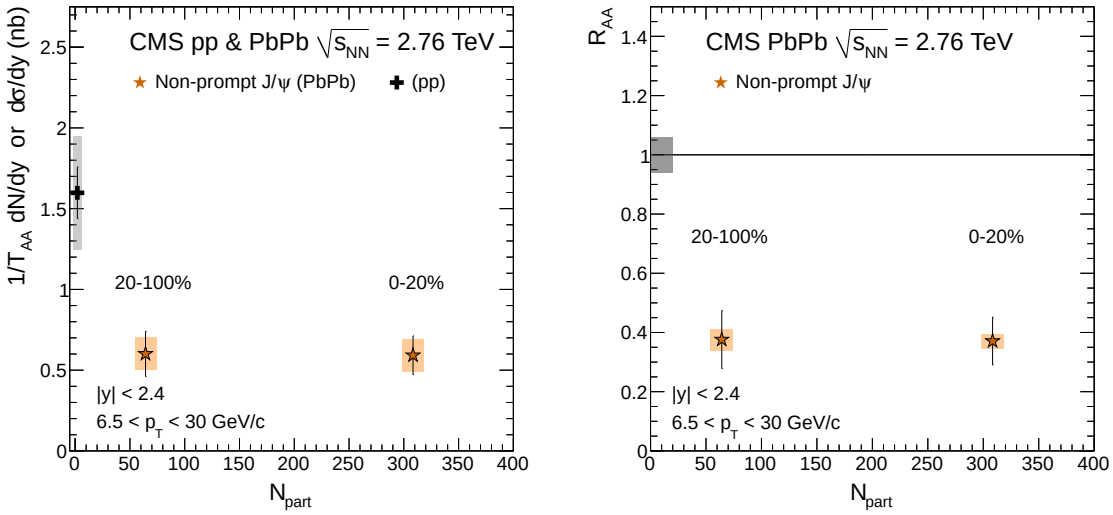

Figure 14: Left: non-prompt J/ψ yield divided by T_{AA} (orange stars) as a function of $N_{\rm part}$ compared to the non-prompt J/ψ cross section measured in pp (black cross). Right: nuclear modification factor R_{AA} of non-prompt J/ψ as a function of $N_{\rm part}$. A global uncertainty of 6%, from the integrated luminosity of the pp data sample, is shown as a grey box at $R_{AA} = 1$. Statistical (systematic) uncertainties are shown as bars (boxes).

conclusions on any p_T or rapidity dependence. The $\Upsilon(1S)$ yield in PbPb collisions divided by T_{AA} and the $\Upsilon(1S)$ R_{AA} are presented as a function of N_{part} in the left and right panels of Fig. 17, respectively. Within uncertainties, no centrality dependence of the $\Upsilon(1S)$ suppression is observed.

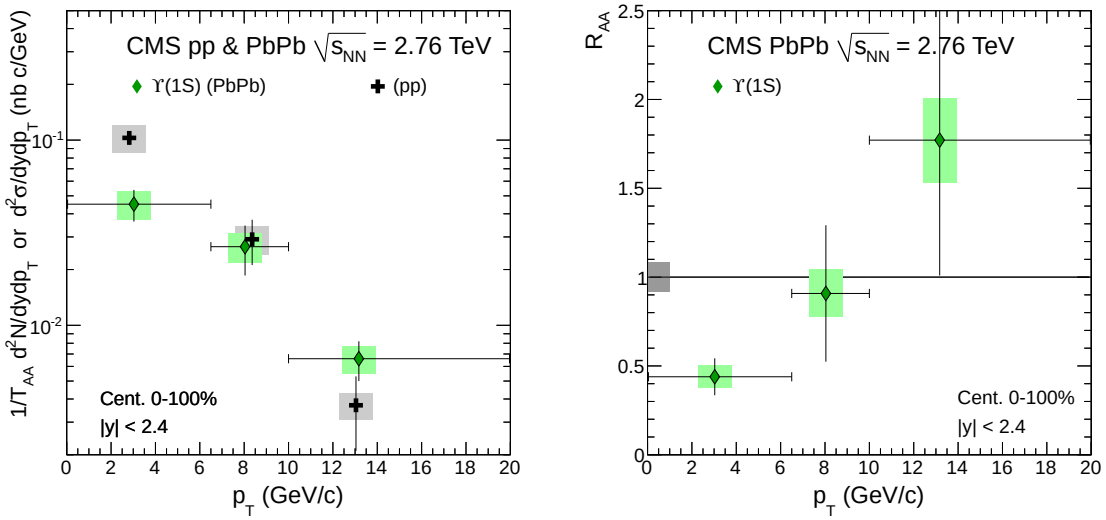

Figure 15: Left: $\Upsilon(1S)$ yield divided by T_{AA} in PbPb collisions (green diamonds) as a function of p_T. The result is compared to the cross section measured in pp collisions (black crosses). The global scale uncertainties on the PbPb data due to T_{AA} (5.7%) and the pp integrated luminosity (6.0%) are not shown. Right: nuclear modification factor R_{AA} of $\Upsilon(1S)$ as a function of p_T. A global uncertainty of 8.3%, from T_{AA} and the integrated luminosity of the pp data sample, is shown as a grey box at $R_{AA} = 1$. Points are plotted at their measured average p_T. Statistical (systematic) uncertainties are shown as bars (boxes). Horizontal bars indicate the bin width.

8 Discussion

This paper has presented the first measurements of the prompt and non-prompt J/ψ, as well as the $\Upsilon(1S)$ mesons, via their decays into $\mu^+\mu^-$ pairs in PbPb and pp collisions at $\sqrt{s_{NN}}$ = 2.76 TeV. The results are based on data recorded with the CMS detector from the first LHC PbPb run in 2010, and from a pp run during March 2011 at $\sqrt{s}$ = 2.76 TeV.

The prompt J/ψ cross section shows a factor of two suppression in central PbPb collisions with respect to peripheral collisions for J/ψ with $6.5 < p_T < 30$ GeV/c. With respect to pp, a nuclear modification factor of $R_{AA} = 0.20 \pm 0.03\,(\text{stat.}) \pm 0.01\,(\text{syst.})$ has been measured in the 10% most central collisions. Prompt J/ψ produced in peripheral collisions are already suppressed with respect to pp: $R_{AA} = 0.61 \pm 0.12\,(\text{stat.}) \pm 0.10\,(\text{syst.})$ in the 50–100% centrality bin. While no p_T dependence is observed in the measured p_T range, within uncertainties, less suppression is observed at forward rapidity ($R_{AA} = 0.43 \pm 0.06\,(\text{stat.}) \pm 0.01\,(\text{syst.})$) than at mid-rapidity ($R_{AA} = 0.29 \pm 0.04\,(\text{stat.}) \pm 0.02\,(\text{syst.})$).

A comparison of the R_{AA} centrality dependence to results measured for $p_T < 5$ GeV/c by PHENIX [21] in AuAu collisions at $\sqrt{s_{NN}}$ = 200 GeV shows a similar suppression, despite the different collision energies and kinematic ranges. Integrated over centrality, CMS has measured an inclusive J/ψ nuclear modification factor of $R_{AA} = 0.41 \pm 0.05\,(\text{stat.}) \pm 0.02\,(\text{syst.})$ in the most forward rapidity bin ($1.6 < |y| < 2.4$) in the p_T range $3 < p_T < 30$ GeV/c. This

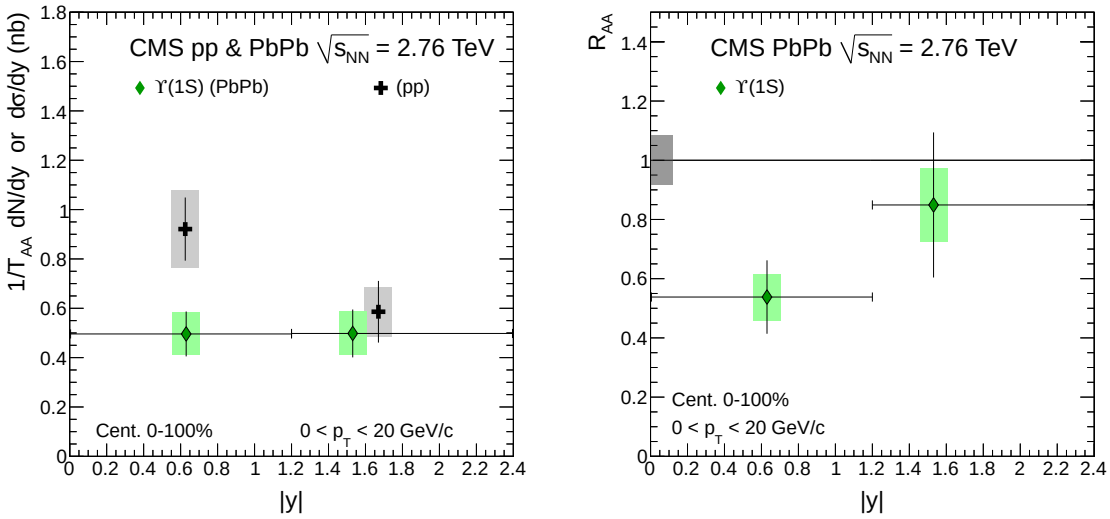

Figure 16: Left: $\Upsilon(1S)$ yield divided by T_{AA} in PbPb collisions (green diamonds) as a function of rapidity. The result is compared to the cross section measured in pp collisions (black crosses). The global scale uncertainties on the PbPb data due to T_{AA} (5.7%) and the pp integrated luminosity (6.0%) are not shown. Right: nuclear modification factor R_{AA} of $\Upsilon(1S)$ as a function of rapidity. A global uncertainty of 8.3%, from T_{AA} and the integrated luminosity of the pp data sample, is shown as a grey box at $R_{AA} = 1$. Points are plotted at their measured average $|y|$. Statistical (systematic) uncertainties are shown as bars (boxes). Horizontal bars indicate the bin width.

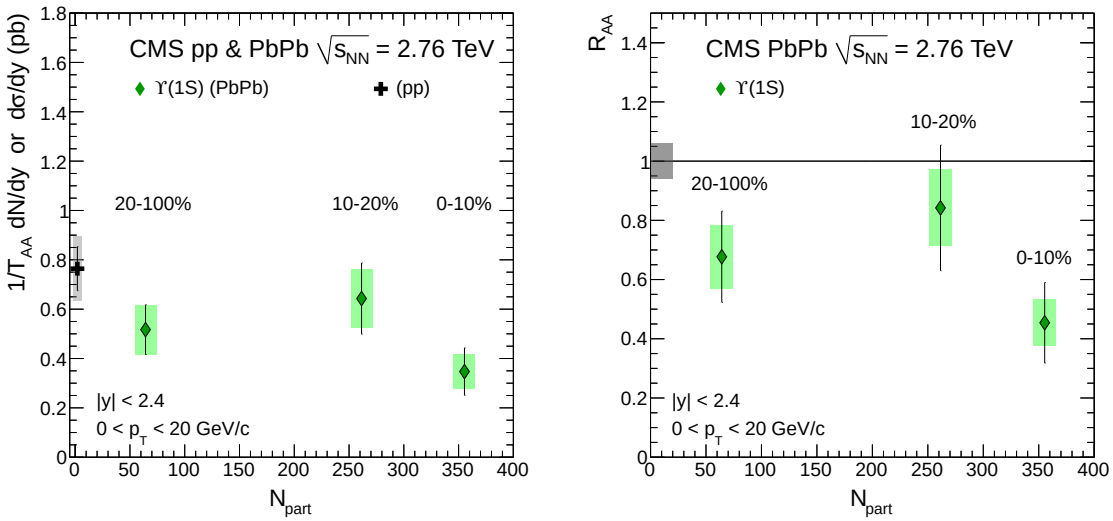

Figure 17: Left: $\Upsilon(1S)$ yield divided by T_{AA} (green diamonds) as a function of N_{part} compared to the $\Upsilon(1S)$ cross section measured in pp (black cross). Right: nuclear modification factor R_{AA} of $\Upsilon(1S)$ as a function of N_{part}. A global uncertainty of 6%, from the integrated luminosity of the pp data sample, is shown as a grey box at $R_{AA} = 1$. Statistical (systematic) uncertainties are shown as bars (boxes).

result is consistent with the ALICE measurement of an inclusive J/ψ R_{AA} of ~ 0.5 at rapidity $2.5 < y < 3.25$ for $p_{\mathrm{T}} > 3\,\mathrm{GeV}/c$ [24].

A strong suppression of non-prompt J/ψ mesons is observed in PbPb collisions when compared to pp collisions. This is the first unambiguous measurement of b-hadron suppression in heavy-ion collisions, which is likely connected to in-medium energy loss of b quarks. The average p_{T} of the non-prompt J/ψ in the measured kinematic range is $\sim 10\,\mathrm{GeV}/c$. Based on simulations of b-hadron decays, this translates into an average b-hadron p_{T} of $\sim 13\,\mathrm{GeV}/c$. The suppression of non-prompt J/ψ is of a comparable magnitude to the charged hadron R_{AA} measured by ALICE [55], which reflects the in-medium energy loss of light quarks. The non-prompt J/ψ yield, though strongly suppressed ($R_{AA} = 0.37 \pm 0.08\,(\mathrm{stat.}) \pm 0.02(\mathrm{syst.})$) in the 20% most central collisions, shows no strong centrality dependence, within uncertainties, when compared to a broad peripheral region (20–100%). Furthermore, this suppression of non-prompt J/ψ is comparable in size to that observed for high-p_{T} single electrons from semileptonic heavy-flavour decays at RHIC [29–31] in which charm and bottom decays were not separated.

The $\Upsilon(1S)$ yield divided by T_{AA} as a function of p_{T}, rapidity, and centrality has been measured in PbPb collisions. No strong centrality dependence is observed within the uncertainties. The nuclear modification factor integrated over centrality is $R_{AA} = 0.63 \pm 0.11\,(\mathrm{stat.}) \pm 0.09\,(\mathrm{syst.})$. This suppression is observed predominantly at low p_{T}. Using $\mathrm{p\overline{p}}$ collisions at $\sqrt{s}$ = 1.8 TeV, CDF measured the fraction of directly produced $\Upsilon(1S)$ as $(50.9 \pm 8.2\,(\mathrm{stat.}) \pm 9.0\,(\mathrm{syst.}))\%$ for $\Upsilon(1S)$ with $p_{\mathrm{T}} > 8\,\mathrm{GeV}/c$ [56]. Therefore, the $\Upsilon(1S)$ suppression presented in this paper could be indirectly caused by the suppression of excited Υ states, as indicated by earlier results from CMS [25].

9 Summary

In summary, CMS has presented the first measurements of prompt J/ψ, non-prompt J/ψ, and $\Upsilon(1S)$ suppression in PbPb collisions at $\sqrt{s_{\mathrm{NN}}}$ = 2.76 TeV. Prompt J/ψ are found to be suppressed, with a strong centrality dependence. By measuring non-prompt J/ψ, CMS has directly observed the suppression of b hadrons for the first time. The measurement of $\Upsilon(1S)$ suppression, together with the suppression of the Υ(2S+3S) states [25], marks the first steps of detailed bottomonium studies in heavy-ion collisions.

Acknowledgements

We wish to congratulate our colleagues in the CERN accelerator departments for the excellent performance of the LHC machine. We thank the technical and administrative staff at CERN and other CMS institutes. This work was supported by the Austrian Federal Ministry of Science and Research; the Belgium Fonds de la Recherche Scientifique, and Fonds voor Wetenschappelijk Onderzoek; the Brazilian Funding Agencies (CNPq, CAPES, FAPERJ, and FAPESP); the Bulgarian Ministry of Education and Science; CERN; the Chinese Academy of Sciences, Ministry of Science and Technology, and National Natural Science Foundation of China; the Colombian Funding Agency (COLCIENCIAS); the Croatian Ministry of Science, Education and Sport; the Research Promotion Foundation, Cyprus; the Estonian Academy of Sciences and NICPB; the Academy of Finland, Finnish Ministry of Education and Culture, and Helsinki Institute of Physics; the Institut National de Physique Nucléaire et de Physique des Particules / CNRS, and Commissariat à l'Énergie Atomique et aux Énergies Alternatives / CEA, France; the Bundesministerium für Bildung und Forschung, Deutsche Forschungsgemeinschaft, and Helmholtz-Gemeinschaft Deutscher Forschungszentren, Germany; the General Secretariat for Research

and Technology, Greece; the National Scientific Research Foundation, and National Office for Research and Technology, Hungary; the Department of Atomic Energy and the Department of Science and Technology, India; the Institute for Studies in Theoretical Physics and Mathematics, Iran; the Science Foundation, Ireland; the Istituto Nazionale di Fisica Nucleare, Italy; the Korean Ministry of Education, Science and Technology and the World Class University program of NRF, Korea; the Lithuanian Academy of Sciences; the Mexican Funding Agencies (CINVESTAV, CONACYT, SEP, and UASLP-FAI); the Ministry of Science and Innovation, New Zealand; the Pakistan Atomic Energy Commission; the Ministry of Science and Higher Education and the National Science Centre, Poland; the Fundação para a Ciência e a Tecnologia, Portugal; JINR (Armenia, Belarus, Georgia, Ukraine, Uzbekistan); the Ministry of Education and Science of the Russian Federation, the Federal Agency of Atomic Energy of the Russian Federation, Russian Academy of Sciences, and the Russian Foundation for Basic Research; the Ministry of Science and Technological Development of Serbia; the Ministerio de Ciencia e Innovación, and Programa Consolider-Ingenio 2010, Spain; the Swiss Funding Agencies (ETH Board, ETH Zurich, PSI, SNF, UniZH, Canton Zurich, and SER); the National Science Council, Taipei; the Scientific and Technical Research Council of Turkey, and Turkish Atomic Energy Authority; the Science and Technology Facilities Council, UK; the US Department of Energy, and the US National Science Foundation.

Individuals have received support from the Marie-Curie programme and the European Research Council (European Union); the Leventis Foundation; the A. P. Sloan Foundation; the Alexander von Humboldt Foundation; the Belgian Federal Science Policy Office; the Fonds pour la Formation à la Recherche dans l'Industrie et dans l'Agriculture (FRIA-Belgium); the Agentschap voor Innovatie door Wetenschap en Technologie (IWT-Belgium); the Council of Science and Industrial Research, India; and the HOMING PLUS programme of Foundation for Polish Science, cofinanced from European Union, Regional Development Fund.

References

[1] F. Karsch and E. Laermann, "Thermodynamics and in-medium hadron properties from lattice QCD", in *Quark-Gluon Plasma III*, R. C. Hwa and X.-N. Wang, eds. World Scientific Publishing Co. Pte. Ltd., 2004. arXiv:hep-lat/0305025.

[2] E. V. Shuryak, "Theory of Hadronic Plasma", *Sov. Phys. JETP* **47** (1978) 212.

[3] BRAHMS Collaboration, "Quark-gluon plasma and color glass condensate at RHIC? The perspective from the BRAHMS experiment", *Nucl. Phys. A* **757** (2005) 1, doi:10.1016/j.nuclphysa.2005.02.130, arXiv:nucl-ex/0410020.

[4] PHOBOS Collaboration, "The PHOBOS perspective on discoveries at RHIC", *Nucl. Phys. A* **757** (2005) 28, doi:10.1016/j.nuclphysa.2005.03.084, arXiv:nucl-ex/0410022.

[5] PHENIX Collaboration, "Formation of dense partonic matter in relativistic nucleus-nucleus collisions at RHIC: Experimental evaluation by the PHENIX Collaboration", *Nucl. Phys. A* **757** (2005) 184, doi:10.1016/j.nuclphysa.2005.03.086, arXiv:nucl-ex/0410003.

[6] STAR Collaboration, "Experimental and theoretical challenges in the search for the quark–gluon plasma: The STAR Collaboration's critical assessment of the evidence from RHIC collisions", *Nucl. Phys. A* **757** (2005) 102, doi:10.1016/j.nuclphysa.2005.03.085, arXiv:nucl-ex/0501009.

[7] T. Matsui and H. Satz, "J/ψ suppression by quark-gluon plasma formation", *Phys. Lett. B* **178** (1986) 416, doi:10.1016/0370-2693(86)91404-8.

[8] Á. Mócsy and P. Petreczky, "Color screening melts quarkonium", *Phys. Rev. Lett.* **99** (2007) 211602, doi:10.1103/PhysRevLett.99.211602, arXiv:0706.2183.

[9] R. Vogt, "Cold Nuclear Matter Effects on J/ψ and Y Production at energies available at the CERN Large Hadron Collider (LHC)", *Phys. Rev. C* **81** (2010) 044903, doi:10.1103/PhysRevC.81.044903, arXiv:1003.3497.

[10] X. Zhao and R. Rapp, "Medium modifications and production of charmonia at LHC", *Nucl. Phys. A* **859** (2011) 114, doi:10.1016/j.nuclphysa.2011.05.001, arXiv:1102.2194.

[11] X. Zhao and R. Rapp, "Charmonium in medium: From correlators to experiment", *Phys. Rev. C* **82** (2010) 064905, doi:10.1103/PhysRevC.82.064905, arXiv:1008.5328.

[12] A. Andronic et al., "Statistical hadronization of heavy quarks in ultra-relativistic nucleus–nucleus collisions", *Nucl. Phys. A* **789** (2007) 334, doi:10.1016/j.nuclphysa.2007.02.013, arXiv:nucl-th/0611023.

[13] A. Capella et al., "Charmonium dissociation and recombination at RHIC and LHC", *Eur. Phys. J. C* **58** (2008) 437, doi:10.1140/epjc/s10052-008-0772-6, arXiv:0712.4331.

[14] R. L. Thews and M. L. Mangano, "Momentum spectra of charmonium produced in a quark-gluon plasma", *Phys. Rev. C* **73** (2006) 014904, doi:10.1103/PhysRevC.73.014904, arXiv:nucl-th/0505055.

[15] L. Yan, P. Zhuang, and N. Xu, "J/ψ production in quark-gluon plasma", *Phys. Rev. Lett.* **97** (2006) 232301, doi:10.1103/PhysRevLett.97.232301, arXiv:nucl-th/0608010.

[16] L. Grandchamp et al., "Bottomonium production at $\sqrt{s_{\rm NN}}$ = 200 GeV and $\sqrt{s_{\rm NN}}$ = 5.5 TeV", *Phys. Rev. C* **73** (2006) 064906, doi:10.1103/PhysRevC.73.064906, arXiv:hep-ph/0507314.

[17] NA38 Collaboration, "ψ' and J/ψ production in pW, pU and SU interactions at 200 GeV/nucleon", *Phys. Lett. B* **345** (1995) 617, doi:10.1016/0370-2693(94)01614-I.

[18] NA50 Collaboration, "A new measurement of J/ψ suppression in PbPb collisions at 158 GeV per nucleon", *Eur. Phys. J. C* **39** (2005) 335, doi:10.1140/epjc/s2004-02107-9, arXiv:hep-ex/0412036.

[19] NA50 Collaboration, "ψ' production in PbPb collisions at 158 GeV/nucleon", *Eur. Phys. J. C* **49** (2007) 559, doi:10.1140/epjc/s10052-006-0153-y, arXiv:nucl-ex/0612013.

[20] NA60 Collaboration, "J/ψ production in InIn collisions at 158 GeV/nucleon", *Phys. Rev. Lett.* **99** (2007) 132302, doi:10.1103/PhysRevLett.99.132302.

[21] PHENIX Collaboration, "J/ψ production versus centrality, transverse momentum, and rapidity in AuAu collisions at $\sqrt{s_{\rm NN}}$ = 200 GeV", *Phys. Rev. Lett.* **98** (2007) 232301, doi:10.1103/PhysRevLett.98.232301, arXiv:nucl-ex/0611020.

[22] STAR Collaboration, "Y cross section in pp collisions at $\sqrt{s}$ = 200 GeV", *Phys. Rev. D* **82** (2010) 012004, doi:10.1103/PhysRevD.82.012004, arXiv:1001.2745.

[23] ATLAS Collaboration, "Measurement of the centrality dependence of J/ψ yields and observation of Z production in PbPb collisions with the ATLAS detector at the LHC", *Phys. Lett. B* **697** (2011) 294, doi:10.1016/j.physletb.2011.02.006, arXiv:1012.5419.

[24] ALICE Collaboration, "J/ψ production at low transverse momentum in PbPb collisions at $\sqrt{s_{\rm NN}}$ = 2.76 TeV", arXiv:1202.1383. submitted to Phys. Rev. Lett.

[25] CMS Collaboration, "Indications of suppression of excited Y states in PbPb collisions at $\sqrt{s_{\rm NN}}$ = 2.76 TeV", *Phys. Rev. Lett.* **107** (2011) 052302, doi:10.1103/PhysRevLett.107.052302, arXiv:1105.4894.

[26] LHCb Collaboration, "Measurement of J/ψ production in pp collisions at $\sqrt{s}$ = 7 TeV", *Eur. Phys. J. C* **71** (2011) 1645, doi:10.1140/epjc/s10052-011-1645-y, arXiv:1103.0423.

[27] CMS Collaboration, "Prompt and non-prompt J/ψ production in pp collisions at $\sqrt{s}$ = 7 TeV", *Eur. Phys. J. C* **71** (2011) 1575, doi:10.1140/epjc/s10052-011-1575-8, arXiv:1011.4193.

[28] ATLAS Collaboration, "Measurement of the differential cross-sections of inclusive, prompt and non-prompt J/ψ production in pp collisions at $\sqrt{s}$ = 7 TeV", *Nucl. Phys. B* **850** (2011) 387, doi:10.1016/j.nuclphysb.2011.05.015, arXiv:1104.3038.

[29] PHENIX Collaboration, "Energy loss and flow of heavy quarks in AuAu collisions at $\sqrt{s_{\rm NN}}$ = 200 GeV", *Phys. Rev. Lett.* **98** (2007) 172301, doi:10.1103/PhysRevLett.98.172301, arXiv:nucl-ex/0611018.

[30] STAR Collaboration, "Transverse momentum and centrality dependence of high-$p_{\rm T}$ nonphotonic electron suppression in AuAu collisions at $\sqrt{s_{\rm NN}}$ = 200 GeV", *Phys. Rev. Lett.* **98** (2007) 192301, doi:10.1103/PhysRevLett.98.192301, arXiv:nucl-ex/0607012v2.

[31] STAR Collaboration, "Erratum: Transverse momentum and centrality dependence of high-$p_{\rm T}$ nonphotonic electron suppression in AuAu collisions at $\sqrt{s_{\rm NN}}$ = 200 GeV", *Phys. Rev. Lett.* **106** (2011) 159902(E), doi:10.1103/PhysRevLett.106.159902, arXiv:nucl-ex/0607012v3.

[32] Y. L. Dokshitzer and D. Kharzeev, "Heavy quark colorimetry of QCD matter", *Phys. Lett. B* **519** (2001) 199, doi:10.1016/S0370-2693(01)01130-3, arXiv:hep-ph/0106202.

[33] N. Armesto et al., "Testing the color charge and mass dependence of parton energy loss with heavy-to-light ratios at BNL RHIC and CERN LHC", *Phys. Rev. D* **71** (2005) 054027, doi:10.1103/PhysRevD.71.054027, arXiv:hep-ph/0501225.

[34] S. Peigne and A. Peshier, "Collisional energy loss of a fast heavy quark in a quark-gluon plasma", *Phys. Rev. D* **77** (2008) 114017, doi:10.1103/PhysRevD.77.114017, arXiv:0802.4364.

[35] CMS Collaboration, "The CMS experiment at the CERN LHC", *JINST* **3** (2008) S08004, doi:10.1088/1748-0221/3/08/S08004.

[36] CMS Collaboration, "Measurement of momentum scale and resolution using low-mass resonances and cosmic ray muons", CMS Physics Analysis Summary TRK-2010/004, (2010).

[37] CMS Collaboration, "Observation and studies of jet quenching in PbPb collisions at $\sqrt{s_{\mathrm{NN}}}$ = 2.76 TeV", *Phys. Rev. C* **84** (2011) 024906, doi:10.1103/PhysRevC.84.024906, arXiv:1102.1957.

[38] CMS Collaboration, "Dependence on pseudorapidity and centrality of charged hadron production in PbPb collisions at $\sqrt{s_{\mathrm{NN}}}$ = 2.76 TeV", *JHEP* **08** (2011) 141, doi:10.1007/JHEP08(2011)141, arXiv:1107.4800.

[39] M. L. Miller et al., "Glauber modeling in high-energy nuclear collisions", *Ann. Rev. Nucl. Part. Sci.* **57** (2007) 205, doi:10.1146/annurev.nucl.57.090506.123020, arXiv:nucl-ex/0701025.

[40] T. Sjöstrand, S. Mrenna, and P. Z. Skands, "PYTHIA 6.4 physics and manual", *JHEP* **05** (2006) 026, doi:10.1088/1126-6708/2006/05/026, arXiv:hep-ph/0603175.

[41] M. Bargiotti and V. Vagnoni, "Heavy quarkonia sector in PYTHIA 6.324: Tuning, validation and perspectives at LHCb", LHCb Note LHCb-2007-042, (2007).

[42] CDF Collaboration, "Measurement of the J/ψ meson and b-hadron production cross sections in $\mathrm{p\overline{p}}$ collisions at $\sqrt{s}$ = 1960 GeV", *Phys. Rev. D* **71** (2005) 032001, doi:10.1103/PhysRevD.71.032001, arXiv:hep-ex/0412071.

[43] D. J. Lange, "The EvtGen particle decay simulation package", *Nucl. Instrum. Meth. A* **462** (2001) 152, doi:10.1016/S0168-9002(01)00089-4.

[44] E. Barberio and Z. Was, "PHOTOS — A universal Monte Carlo for QED radiative corrections: version 2.0", *Comput. Phys. Commun.* **79** (1994) 291, doi:10.1016/0010-4655(94)90074-4.

[45] GEANT Collaboration, "GEANT4 — A simulation toolkit", *Nucl. Instrum. Meth. A* **506** (2003) 250, doi:10.1016/S0168-9002(03)01368-8.

[46] I. P. Lokhtin and A. M. Snigirev, "A model of jet quenching in ultrarelativistic heavy ion collisions and high-p_{T} hadron spectra at RHIC", *Eur. Phys. J. C* **45** (2006) 211, doi:10.1140/epjc/s2005-02426-3, arXiv:hep-ph/0506189.

[47] CMS Collaboration, "CMS physics technical design report: Addendum on high density QCD with heavy ions", *J. Phys. G* **34** (2007) 2307, doi:10.1088/0954-3899/34/11/008.

[48] C. Roland (on behalf of the CMS Collaboration), "Track reconstruction in heavy ion collisions with the CMS silicon tracker", *Nucl. Instrum. Meth. A* **566** (2006) 123, doi:10.1016/j.nima.2006.05.023.

[49] Particle Data Group Collaboration, "Review of particle physics", *J. Phys. G* **37** (2010) 075021, doi:10.1088/0954-3899/37/7A/075021.

[50] ALICE Collaboration, "ALICE: Physics performance report, volume II", *J. Phys. G* **32** (2006) 1295, doi:10.1088/0954-3899/32/10/001.

[51] ALEPH Collaboration, "Measurement of the $\overline{\mathrm{B}}^0$ and B^- meson lifetimes", *Phys. Lett. B* **307** (1993) 194, doi:10.1016/0370-2693(93)90211-Y.

[52] ALEPH Collaboration, "Errata: Measurement of the $\overline{\mathrm{B}}^0$ and B^- meson lifetimes", *Phys. Lett. B* **325** (1994) 537, doi:10.1016/0370-2693(94)90054-X.

[53] CMS Collaboration, "Performance of muon identification in pp collisions at $\sqrt{s} = 7$ TeV", CMS Physics Analysis Summary MUO-2010/02, (2010).

[54] P. Faccioli and J. Seixas, "Observation of χ_c and χ_b nuclear suppression via dilepton polarization measurements", arXiv:1203.2033.

[55] ALICE Collaboration, "Suppression of charged particle production at large transverse momentum in central PbPb Collisions at $\sqrt{s_{\mathrm{NN}}} = 2.76$ TeV", *Phys. Lett. B* **696** (2011) 30, doi:10.1016/j.physletb.2010.12.020, arXiv:1012.1004.

[56] CDF Collaboration, "Production of $\Upsilon(1S)$ mesons from χ_b decays in $\mathrm{p\overline{p}}$ collisions at $\sqrt{s} = 1.8$ TeV", *Phys. Rev. Lett.* **84** (2000) 2094, doi:10.1103/PhysRevLett.84.2094, arXiv:hep-ex/9910025.

A Tables of Results

Table 4: Raw yield of inclusive J/ψ as a function of J/ψ rapidity and p_{T} in PbPb and pp collisions. For PbPb, the raw yield is also included as a function of collision centrality. All quoted uncertainties are statistical.

$\lvert y\rvert$	p_{T} [GeV/c]	centrality	Raw yield PbPb	Raw yield pp
0.0–2.4	6.5–30	0–100%	396 ± 24	1026 ± 35
	6.5–10		261 ± 20	684 ± 30
	10–30		138 ± 14	342 ± 19
0.0–1.2	6.5–30	0–100%	174 ± 16	462 ± 36
1.2–1.6	5.5–30	0–100%	103 ± 13	360 ± 23
	6.5–30		90 ± 11	272 ± 21
1.6–2.4	3.0–30	0–100%	446 ± 56	1006 ± 34
	6.5–30		150 ± 15	329 ± 19
0.0–2.4	6.5–30	0–10%	113 ± 12	
		10–20%	80 ± 10	
		20–30%	63 ± 9	
		30–40%	58 ± 8	
		40–50%	45 ± 7	
		50–100%	37 ± 6	
		0–20%	193 ± 16	
		20–100%	205 ± 15	

Table 5: Raw yield of $\Upsilon(1S)$ as a function of $\Upsilon(1S)$ rapidity and p_T in PbPb and pp collisions. For PbPb, the raw yield is also included as a function of collision centrality. All quoted uncertainties are statistical.

$\lvert y\rvert$	p_T [GeV/c]	centrality	Raw yield PbPb	Raw yield pp
0.0–2.4	0–6.5	0–100%	44 ± 9	75 ± 10
	6.5–10		18 ± 5	15 ± 5
	10–20		24 ± 6	10 ± 4
	0–20		86 ± 12	101 ± 12
0.0–1.2	0–20	0–100%	48 ± 9	66 ± 9
1.2–2.4			40 ± 8	34 ± 7
0.0–2.4	0–20	0–10%	24 ± 7	
		10–20%	30 ± 7	
		20–100%	32 ± 6	
		0–20%	54 ± 9	

Table 6: Yield per unit of rapidity of inclusive J/ψ divided by T_{AA} and nuclear modification factor R_{AA} as a function of J/ψ rapidity, p_T, and collision centrality. The average p_T value for each bin is given. Listed uncertainties are statistical first, systematic second, and global scale third. The latter includes the uncertainties on the pp integrated luminosity and, for centrality integrated bins, on T_{AA}.

$\lvert y\rvert$	p_T [GeV/c]	centrality	$\langle p_T \rangle$ [GeV/c]	$\frac{1}{T_{AA}} \cdot \frac{dN}{dy}$ [nb]	R_{AA}
0.0–2.4	6.5–30	0–100%	9.87	$2.40 \pm 0.15 \pm 0.34 \pm 0.14$	$0.32 \pm 0.02 \pm 0.01 \pm 0.03$
	6.5–10		8.11	$2.05 \pm 0.15 \pm 0.30 \pm 0.12$	$0.32 \pm 0.03 \pm 0.02 \pm 0.03$
	10–30		13.22	$0.40 \pm 0.04 \pm 0.06 \pm 0.02$	$0.31 \pm 0.04 \pm 0.01 \pm 0.03$
0.0–1.2	6.5–30	0–100%	10.92	$2.76 \pm 0.26 \pm 0.43 \pm 0.16$	$0.29 \pm 0.04 \pm 0.02 \pm 0.02$
1.2–1.6	5.5–30	0–100%	9.21	$3.57 \pm 0.45 \pm 0.51 \pm 0.20$	$0.23 \pm 0.03 \pm 0.02 \pm 0.02$
	6.5–30		9.65	$2.29 \pm 0.28 \pm 0.33 \pm 0.13$	$0.28 \pm 0.04 \pm 0.02 \pm 0.02$
1.6–2.4	3.0–30	0–100%	6.27	$21.18 \pm 2.65 \pm 3.18 \pm 1.21$	$0.41 \pm 0.05 \pm 0.02 \pm 0.03$
	6.5–30		8.92	$2.22 \pm 0.21 \pm 0.32 \pm 0.13$	$0.40 \pm 0.05 \pm 0.01 \pm 0.03$
0.0–2.4	6.5–30	0–10%	10.39	$1.78 \pm 0.20 \pm 0.27$	$0.24 \pm 0.03 \pm 0.02 \pm 0.01$
		10–20%	9.70	$1.92 \pm 0.24 \pm 0.30$	$0.26 \pm 0.03 \pm 0.02 \pm 0.02$
		20–30%	10.23	$2.37 \pm 0.33 \pm 0.38$	$0.31 \pm 0.04 \pm 0.02 \pm 0.02$
		30–40%	9.27	$3.73 \pm 0.53 \pm 0.63$	$0.50 \pm 0.07 \pm 0.05 \pm 0.03$
		40–50%	9.29	$5.22 \pm 0.81 \pm 0.95$	$0.70 \pm 0.11 \pm 0.08 \pm 0.04$
		50–100%	9.64	$4.67 \pm 0.80 \pm 0.97$	$0.62 \pm 0.11 \pm 0.10 \pm 0.04$
		0–20%	9.27	$1.84 \pm 0.15 \pm 0.28$	$0.25 \pm 0.02 \pm 0.02 \pm 0.02$
		20–100%	9.29	$3.46 \pm 0.26 \pm 0.58$	$0.46 \pm 0.04 \pm 0.04 \pm 0.03$

Table 7: Yield per unit of rapidity of prompt J/ψ divided by T_{AA} and nuclear modification factor R_{AA} as a function of J/ψ rapidity, p_{T}, and collision centrality. The average p_{T} value for each bin is given. Listed uncertainties are statistical first, systematic second, and global scale third. The latter includes the uncertainties on the pp integrated luminosity and, for centrality integrated bins, on T_{AA}.

$\lvert y\rvert$	p_{T} [GeV/c]	centrality	$\langle p_{\mathrm{T}}\rangle$ [GeV/c]	$\frac{1}{T_{AA}}\cdot\frac{\mathrm{d}N}{\mathrm{d}y}$ [nb]	R_{AA}
0.0–2.4	6.5–30	0–100%	9.87	$1.79 \pm 0.13 \pm 0.26 \pm 0.10$	$0.30 \pm 0.03 \pm 0.01 \pm 0.02$
	6.5–10		8.11	$1.56 \pm 0.14 \pm 0.23 \pm 0.09$	$0.30 \pm 0.03 \pm 0.02 \pm 0.02$
	10–30		13.22	$0.27 \pm 0.03 \pm 0.04 \pm 0.02$	$0.31 \pm 0.04 \pm 0.01 \pm 0.03$
0.0–1.2	6.5–30	0–100%	10.92	$2.11 \pm 0.23 \pm 0.32 \pm 0.12$	$0.29 \pm 0.04 \pm 0.02 \pm 0.02$
1.2–1.6	5.5–30	0–100%	9.21	$2.95 \pm 0.44 \pm 0.45 \pm 0.17$	$0.24 \pm 0.04 \pm 0.02 \pm 0.02$
	6.5–30		9.65	$1.71 \pm 0.25 \pm 0.24 \pm 0.10$	$0.27 \pm 0.05 \pm 0.02 \pm 0.02$
1.6–2.4	3.0–30	0–100%	6.27	$17.78 \pm 2.35 \pm 2.60 \pm 1.01$	$0.40 \pm 0.05 \pm 0.02 \pm 0.03$
	6.5–30		8.92	$1.83 \pm 0.20 \pm 0.26 \pm 0.10$	$0.43 \pm 0.06 \pm 0.01 \pm 0.04$
0.0–2.4	6.5–30	0–10%	10.39	$1.18 \pm 0.17 \pm 0.18$	$0.20 \pm 0.03 \pm 0.01 \pm 0.01$
		10–20%	9.70	$1.29 \pm 0.21 \pm 0.20$	$0.22 \pm 0.04 \pm 0.02 \pm 0.01$
		20–30%	10.23	$2.18 \pm 0.33 \pm 0.35$	$0.37 \pm 0.06 \pm 0.03 \pm 0.02$
		30–40%	9.27	$2.97 \pm 0.48 \pm 0.50$	$0.51 \pm 0.09 \pm 0.05 \pm 0.03$
		40–50%	9.29	$3.88 \pm 0.75 \pm 0.70$	$0.66 \pm 0.13 \pm 0.08 \pm 0.04$
		50–100%	9.64	$3.58 \pm 0.70 \pm 0.75$	$0.61 \pm 0.12 \pm 0.10 \pm 0.04$
		0–20%	9.27	$1.23 \pm 0.14 \pm 0.19$	$0.21 \pm 0.02 \pm 0.01 \pm 0.01$
		20–100%	9.29	$2.84 \pm 0.25 \pm 0.47$	$0.48 \pm 0.05 \pm 0.05 \pm 0.01$

Table 8: Yield per unit of rapidity of non-prompt J/ψ divided by T_{AA} and nuclear modification factor R_{AA} as a function of J/ψ rapidity, p_{T}, and collision centrality. The average p_{T} value for each bin is given. Listed uncertainties are statistical first, systematic second, and global scale third. The latter includes the uncertainties on the pp integrated luminosity and, for centrality integrated bins, on T_{AA}.

$\lvert y\rvert$	p_{T} [GeV/c]	centrality	$\langle p_{\mathrm{T}}\rangle$ [GeV/c]	$\frac{1}{T_{AA}}\cdot\frac{\mathrm{d}N}{\mathrm{d}y}$ [nb]	R_{AA}
0.0–2.4	6.5–30	0–100%	9.87	$0.60 \pm 0.09 \pm 0.09 \pm 0.03$	$0.38 \pm 0.07 \pm 0.02 \pm 0.03$
1.6–2.4	3.0–30	0–100%	6.27	$3.29 \pm 0.82 \pm 0.65 \pm 0.19$	$0.50 \pm 0.14 \pm 0.02 \pm 0.04$
	6.5–30		8.92	$0.39 \pm 0.12 \pm 0.06 \pm 0.02$	$0.31 \pm 0.11 \pm 0.01 \pm 0.03$
0.0–2.4	6.5–30	0–20%	9.27	$0.59 \pm 0.12 \pm 0.10$	$0.37 \pm 0.08 \pm 0.02 \pm 0.02$
		20–100%	9.29	$0.60 \pm 0.14 \pm 0.10$	$0.38 \pm 0.10 \pm 0.04 \pm 0.02$

Table 9: Yield per unit of rapidity of Υ(1S) divided by T_{AA} and nuclear modification factor R_{AA} as a function of Υ(1S) rapidity, p_{T}, and collision centrality. The average p_{T} value for each bin is given. Listed uncertainties are statistical first, systematic second, and global scale third. The latter includes the uncertainties on the pp integrated luminosity and, for centrality integrated bins, on T_{AA}.

$\lvert y\rvert$	p_{T} [GeV/c]	centrality	$\langle p_{\mathrm{T}}\rangle$ [GeV/c]	$\frac{1}{T_{AA}}\cdot\frac{\mathrm{d}N}{\mathrm{d}y}$ [nb]	R_{AA}
0.0–2.4	0–6.5	0–100%	3.03	$0.293 \pm 0.057 \pm 0.051 \pm 0.02$	$0.44 \pm 0.10 \pm 0.06 \pm 0.04$
	6.5–10		8.04	$0.093 \pm 0.028 \pm 0.017 \pm 0.01$	$0.91 \pm 0.38 \pm 0.13 \pm 0.08$
	10–20		13.17	$0.066 \pm 0.016 \pm 0.011 \pm 0.004$	$1.77 \pm 0.76 \pm 0.24 \pm 0.15$
	0–20		6.79	$0.485 \pm 0.066 \pm 0.084 \pm 0.03$	$0.63 \pm 0.11 \pm 0.09 \pm 0.05$
0.0–1.2	0–20	0–100%	6.44	$0.495 \pm 0.091 \pm 0.086 \pm 0.03$	$0.54 \pm 0.12 \pm 0.08 \pm 0.04$
1.2–2.4			6.60	$0.498 \pm 0.097 \pm 0.088 \pm 0.03$	$0.85 \pm 0.25 \pm 0.12 \pm 0.07$
0.0–2.4	0–20	0–10%	6.65	$0.347 \pm 0.096 \pm 0.069$	$0.45 \pm 0.14 \pm 0.08 \pm 0.03$
		10–20%	6.88	$0.643 \pm 0.144 \pm 0.118$	$0.84 \pm 0.21 \pm 0.13 \pm 0.05$
		20–100%	6.08	$0.517 \pm 0.101 \pm 0.101$	$0.68 \pm 0.15 \pm 0.11 \pm 0.04$
		0–20%	6.85	$0.467 \pm 0.081 \pm 0.093$	$0.61 \pm 0.13 \pm 0.11 \pm 0.04$

Table 10: Cross section per unit of rapidity of inclusive J/ψ as a function of rapidity and p_{T} in pp collisions. The average p_{T} value for each bin is given. Listed uncertainties are statistical first, systematic second, and global scale third. The latter is the uncertainty on the pp integrated luminosity.

$\lvert y\rvert$	p_{T} [GeV/c]	$\langle p_{\mathrm{T}}\rangle$ [GeV/c]	$\frac{\mathrm{d}\sigma}{\mathrm{d}y}$ [nb]
0.0–2.4	6.5–30	9.82	$7.50 \pm 0.26 \pm 1.10 \pm 0.45$
	6.5–10	8.05	$6.37 \pm 0.28 \pm 0.99 \pm 0.38$
	10–30	13.34	$1.27 \pm 0.07 \pm 0.18 \pm 0.08$
0.0–1.2	6.5–30	10.81	$9.45 \pm 0.74 \pm 1.38 \pm 0.57$
1.2–1.6	5.5–30	8.53	$15.22 \pm 0.96 \pm 2.23 \pm 0.91$
	6.5–30	9.31	$8.27 \pm 0.64 \pm 1.23 \pm 0.50$
1.6–2.4	3.0–30	6.15	$51.52 \pm 1.74 \pm 7.33 \pm 3.09$
	6.5–30	8.98	$5.54 \pm 0.33 \pm 0.79 \pm 0.33$

Table 11: Cross section per unit of rapidity of prompt J/ψ as a function of rapidity, p_{T} in pp collisions. The average p_{T} value for each bin is given. Listed uncertainties are statistical first, systematic second, and global scale third. The latter is the uncertainty on the pp integrated luminosity.

$\lvert y\rvert$	p_{T} [GeV/c]	$\langle p_{\mathrm{T}}\rangle$ [GeV/c]	$\frac{\mathrm{d}\sigma}{\mathrm{d}y}$ [nb]
0.0–2.4	6.5–30	9.82	$5.87 \pm 0.24 \pm 0.86 \pm 0.35$
	6.5–10	8.05	$5.14 \pm 0.26 \pm 0.80 \pm 0.31$
	10–30	13.34	$0.89 \pm 0.06 \pm 0.12 \pm 0.05$
0.0–1.2	6.5–30	10.81	$7.40 \pm 0.64 \pm 1.08 \pm 0.44$
1.2–1.6	5.5–30	8.53	$12.38 \pm 0.92 \pm 1.81 \pm 0.74$
	6.5–30	9.31	$6.39 \pm 0.57 \pm 0.95 \pm 0.38$
1.6–2.4	3.0–30	6.15	$44.67 \pm 1.78 \pm 6.35 \pm 2.68$
	6.5–30	8.98	$4.26 \pm 0.31 \pm 0.61 \pm 0.26$

Table 12: Cross section per unit of rapidity of non-prompt J/ψ as a function of rapidity and p_{T} in pp collisions. The average p_{T} value for each bin is given. Listed uncertainties are statistical first, systematic second, and global scale third. The latter is the uncertainty on the pp integrated luminosity.

$\lvert y\rvert$	p_{T} [GeV/c]	$\langle p_{\mathrm{T}}\rangle$ [GeV/c]	$\frac{\mathrm{d}\sigma}{\mathrm{d}y}$ [nb]
0.0–2.4	6.5–30	9.82	$1.60 \pm 0.16 \pm 0.35 \pm 0.10$
1.6–2.4	3.0–30	6.15	$6.61 \pm 0.93 \pm 0.98 \pm 0.40$
	6.5–30	8.98	$1.25 \pm 0.21 \pm 0.19 \pm 0.08$

Table 13: Cross section per unit of rapidity of $\Upsilon(1S)$ as a function of rapidity and p_{T} in pp collisions. The average p_{T} value for each bin is given. Listed uncertainties are statistical first, systematic second, and global scale third. The latter is the uncertainty on the pp integrated luminosity.

$\lvert y\rvert$	p_{T} [GeV/c]	$\langle p_{\mathrm{T}}\rangle$ [GeV/c]	$\frac{\mathrm{d}\sigma}{\mathrm{d}y}$ [nb]
0.0–2.4	0–6.5	2.82	$0.668 \pm 0.091 \pm 0.115 \pm 0.040$
	6.5–10	8.36	$0.102 \pm 0.031 \pm 0.018 \pm 0.006$
	10–20	13.04	$0.037 \pm 0.013 \pm 0.006 \pm 0.002$
	0–20	4.73	$0.764 \pm 0.089 \pm 0.131 \pm 0.046$
0.0–1.2	0–20	5.18	$0.921 \pm 0.128 \pm 0.157 \pm 0.055$
1.2–2.4		4.03	$0.586 \pm 0.125 \pm 0.101 \pm 0.035$

B The CMS Collaboration

Yerevan Physics Institute, Yerevan, Armenia
S. Chatrchyan, V. Khachatryan, A.M. Sirunyan, A. Tumasyan

Institut für Hochenergiephysik der OeAW, Wien, Austria
W. Adam, T. Bergauer, M. Dragicevic, J. Erö, C. Fabjan, M. Friedl, R. Frühwirth, V.M. Ghete, J. Hammer[1], M. Hoch, N. Hörmann, J. Hrubec, M. Jeitler, W. Kiesenhofer, M. Krammer, D. Liko, I. Mikulec, M. Pernicka[†], B. Rahbaran, C. Rohringer, H. Rohringer, R. Schöfbeck, J. Strauss, A. Taurok, F. Teischinger, P. Wagner, W. Waltenberger, G. Walzel, E. Widl, C.-E. Wulz

National Centre for Particle and High Energy Physics, Minsk, Belarus
V. Mossolov, N. Shumeiko, J. Suarez Gonzalez

Universiteit Antwerpen, Antwerpen, Belgium
S. Bansal, L. Benucci, E.A. De Wolf, X. Janssen, S. Luyckx, T. Maes, L. Mucibello, S. Ochesanu, B. Roland, R. Rougny, M. Selvaggi, H. Van Haevermaet, P. Van Mechelen, N. Van Remortel, A. Van Spilbeeck

Vrije Universiteit Brussel, Brussel, Belgium
F. Blekman, S. Blyweert, J. D'Hondt, R. Gonzalez Suarez, A. Kalogeropoulos, M. Maes, A. Olbrechts, W. Van Doninck, P. Van Mulders, G.P. Van Onsem, I. Villella

Université Libre de Bruxelles, Bruxelles, Belgium
O. Charaf, B. Clerbaux, G. De Lentdecker, V. Dero, A.P.R. Gay, G.H. Hammad, T. Hreus, A. Léonard, P.E. Marage, L. Thomas, C. Vander Velde, P. Vanlaer, J. Wickens

Ghent University, Ghent, Belgium
V. Adler, K. Beernaert, A. Cimmino, S. Costantini, M. Grunewald, B. Klein, J. Lellouch, A. Marinov, J. Mccartin, D. Ryckbosch, N. Strobbe, F. Thyssen, M. Tytgat, L. Vanelderen, P. Verwilligen, S. Walsh, N. Zaganidis

Université Catholique de Louvain, Louvain-la-Neuve, Belgium
S. Basegmez, G. Bruno, J. Caudron, L. Ceard, J. De Favereau De Jeneret, C. Delaere, D. Favart, L. Forthomme, A. Giammanco[2], G. Grégoire, J. Hollar, V. Lemaitre, J. Liao, O. Militaru, C. Nuttens, D. Pagano, A. Pin, K. Piotrzkowski, N. Schul

Université de Mons, Mons, Belgium
N. Beliy, T. Caebergs, E. Daubie

Centro Brasileiro de Pesquisas Fisicas, Rio de Janeiro, Brazil
G.A. Alves, D. De Jesus Damiao, M.E. Pol, M.H.G. Souza

Universidade do Estado do Rio de Janeiro, Rio de Janeiro, Brazil
W.L. Aldá Júnior, W. Carvalho, A. Custódio, E.M. Da Costa, C. De Oliveira Martins, S. Fonseca De Souza, D. Matos Figueiredo, L. Mundim, H. Nogima, V. Oguri, W.L. Prado Da Silva, A. Santoro, S.M. Silva Do Amaral, A. Sznajder

Instituto de Fisica Teorica, Universidade Estadual Paulista, Sao Paulo, Brazil
T.S. Anjos[3], C.A. Bernardes[3], F.A. Dias[4], T.R. Fernandez Perez Tomei, E. M. Gregores[3], C. Lagana, F. Marinho, P.G. Mercadante[3], S.F. Novaes, Sandra S. Padula

Institute for Nuclear Research and Nuclear Energy, Sofia, Bulgaria
N. Darmenov[1], V. Genchev[1], P. Iaydjiev[1], S. Piperov, M. Rodozov, S. Stoykova, G. Sultanov, V. Tcholakov, R. Trayanov, M. Vutova

University of Sofia, Sofia, Bulgaria
A. Dimitrov, R. Hadjiiska, A. Karadzhinova, V. Kozhuharov, L. Litov, B. Pavlov, P. Petkov

Institute of High Energy Physics, Beijing, China
J.G. Bian, G.M. Chen, H.S. Chen, C.H. Jiang, D. Liang, S. Liang, X. Meng, J. Tao, J. Wang, J. Wang, X. Wang, Z. Wang, H. Xiao, M. Xu, J. Zang, Z. Zhang

State Key Lab. of Nucl. Phys. and Tech., Peking University, Beijing, China
Y. Ban, S. Guo, Y. Guo, W. Li, S. Liu, Y. Mao, S.J. Qian, H. Teng, S. Wang, B. Zhu, W. Zou

Universidad de Los Andes, Bogota, Colombia
A. Cabrera, B. Gomez Moreno, A.A. Ocampo Rios, A.F. Osorio Oliveros, J.C. Sanabria

Technical University of Split, Split, Croatia
N. Godinovic, D. Lelas, R. Plestina[5], D. Polic, I. Puljak

University of Split, Split, Croatia
Z. Antunovic, M. Dzelalija, M. Kovac

Institute Rudjer Boskovic, Zagreb, Croatia
V. Brigljevic, S. Duric, K. Kadija, J. Luetic, S. Morovic

University of Cyprus, Nicosia, Cyprus
A. Attikis, M. Galanti, J. Mousa, C. Nicolaou, F. Ptochos, P.A. Razis

Charles University, Prague, Czech Republic
M. Finger, M. Finger Jr.

Academy of Scientific Research and Technology of the Arab Republic of Egypt, Egyptian Network of High Energy Physics, Cairo, Egypt
Y. Assran[6], A. Ellithi Kamel[7], S. Khalil[8], M.A. Mahmoud[9], A. Radi[8]

National Institute of Chemical Physics and Biophysics, Tallinn, Estonia
A. Hektor, M. Kadastik, M. Müntel, M. Raidal, L. Rebane, A. Tiko

Department of Physics, University of Helsinki, Helsinki, Finland
V. Azzolini, P. Eerola, G. Fedi, M. Voutilainen

Helsinki Institute of Physics, Helsinki, Finland
S. Czellar, J. Härkönen, A. Heikkinen, V. Karimäki, R. Kinnunen, M.J. Kortelainen, T. Lampén, K. Lassila-Perini, S. Lehti, T. Lindén, P. Luukka, T. Mäenpää, E. Tuominen, J. Tuominiemi, E. Tuovinen, D. Ungaro, L. Wendland

Lappeenranta University of Technology, Lappeenranta, Finland
K. Banzuzi, A. Karjalainen, A. Korpela, T. Tuuva

Laboratoire d'Annecy-le-Vieux de Physique des Particules, IN2P3-CNRS, Annecy-le-Vieux, France
D. Sillou

DSM/IRFU, CEA/Saclay, Gif-sur-Yvette, France
M. Besancon, S. Choudhury, M. Dejardin, D. Denegri, B. Fabbro, J.L. Faure, F. Ferri, S. Ganjour, A. Givernaud, P. Gras, G. Hamel de Monchenault, P. Jarry, E. Locci, J. Malcles, M. Marionneau, L. Millischer, J. Rander, A. Rosowsky, I. Shreyber, M. Titov

Laboratoire Leprince-Ringuet, Ecole Polytechnique, IN2P3-CNRS, Palaiseau, France
S. Baffioni, F. Beaudette, L. Benhabib, L. Bianchini, M. Bluj[10], C. Broutin, P. Busson, C. Charlot,

N. Daci, T. Dahms, L. Dobrzynski, S. Elgammal, R. Granier de Cassagnac, M. Haguenauer, P. Miné, C. Mironov, C. Ochando, P. Paganini, D. Sabes, R. Salerno, Y. Sirois, C. Thiebaux, C. Veelken, A. Zabi

Institut Pluridisciplinaire Hubert Curien, Université de Strasbourg, Université de Haute Alsace Mulhouse, CNRS/IN2P3, Strasbourg, France
J.-L. Agram[11], J. Andrea, D. Bloch, D. Bodin, J.-M. Brom, M. Cardaci, E.C. Chabert, C. Collard, E. Conte[11], F. Drouhin[11], C. Ferro, J.-C. Fontaine[11], D. Gelé, U. Goerlach, S. Greder, P. Juillot, M. Karim[11], A.-C. Le Bihan, P. Van Hove

Centre de Calcul de l'Institut National de Physique Nucleaire et de Physique des Particules (IN2P3), Villeurbanne, France
F. Fassi, D. Mercier

Université de Lyon, Université Claude Bernard Lyon 1, CNRS-IN2P3, Institut de Physique Nucléaire de Lyon, Villeurbanne, France
C. Baty, S. Beauceron, N. Beaupere, M. Bedjidian, O. Bondu, G. Boudoul, D. Boumediene, H. Brun, J. Chasserat, R. Chierici[1], D. Contardo, P. Depasse, H. El Mamouni, A. Falkiewicz, J. Fay, S. Gascon, B. Ille, T. Kurca, T. Le Grand, M. Lethuillier, L. Mirabito, S. Perries, V. Sordini, S. Tosi, Y. Tschudi, P. Verdier, S. Viret

Institute of High Energy Physics and Informatization, Tbilisi State University, Tbilisi, Georgia
D. Lomidze

RWTH Aachen University, I. Physikalisches Institut, Aachen, Germany
G. Anagnostou, S. Beranek, M. Edelhoff, L. Feld, N. Heracleous, O. Hindrichs, R. Jussen, K. Klein, J. Merz, A. Ostapchuk, A. Perieanu, F. Raupach, J. Sammet, S. Schael, D. Sprenger, H. Weber, M. Weber, B. Wittmer, V. Zhukov[12]

RWTH Aachen University, III. Physikalisches Institut A, Aachen, Germany
M. Ata, E. Dietz-Laursonn, M. Erdmann, T. Hebbeker, C. Heidemann, A. Hinzmann, K. Hoepfner, T. Klimkovich, D. Klingebiel, P. Kreuzer, D. Lanske†, J. Lingemann, C. Magass, M. Merschmeyer, A. Meyer, P. Papacz, H. Pieta, H. Reithler, S.A. Schmitz, L. Sonnenschein, J. Steggemann, D. Teyssier

RWTH Aachen University, III. Physikalisches Institut B, Aachen, Germany
M. Bontenackels, V. Cherepanov, M. Davids, G. Flügge, H. Geenen, W. Haj Ahmad, F. Hoehle, B. Kargoll, T. Kress, Y. Kuessel, A. Linn, A. Nowack, L. Perchalla, O. Pooth, J. Rennefeld, P. Sauerland, A. Stahl, D. Tornier, M.H. Zoeller

Deutsches Elektronen-Synchrotron, Hamburg, Germany
M. Aldaya Martin, W. Behrenhoff, U. Behrens, M. Bergholz[13], A. Bethani, K. Borras, A. Cakir, A. Campbell, E. Castro, D. Dammann, G. Eckerlin, D. Eckstein, A. Flossdorf, G. Flucke, A. Geiser, J. Hauk, H. Jung[1], M. Kasemann, P. Katsas, C. Kleinwort, H. Kluge, A. Knutsson, M. Krämer, D. Krücker, E. Kuznetsova, W. Lange, W. Lohmann[13], B. Lutz, R. Mankel, I. Marfin, M. Marienfeld, I.-A. Melzer-Pellmann, A.B. Meyer, J. Mnich, A. Mussgiller, S. Naumann-Emme, J. Olzem, A. Petrukhin, D. Pitzl, A. Raspereza, M. Rosin, J. Salfeld-Nebgen, R. Schmidt[13], T. Schoerner-Sadenius, N. Sen, A. Spiridonov, M. Stein, J. Tomaszewska, R. Walsh, C. Wissing

University of Hamburg, Hamburg, Germany
C. Autermann, V. Blobel, S. Bobrovskyi, J. Draeger, H. Enderle, U. Gebbert, M. Görner, T. Hermanns, K. Kaschube, G. Kaussen, H. Kirschenmann, R. Klanner, J. Lange, B. Mura,

F. Nowak, N. Pietsch, C. Sander, H. Schettler, P. Schleper, E. Schlieckau, M. Schröder, T. Schum, H. Stadie, G. Steinbrück, J. Thomsen

Institut für Experimentelle Kernphysik, Karlsruhe, Germany
C. Barth, J. Berger, T. Chwalek, W. De Boer, A. Dierlamm, G. Dirkes, M. Feindt, J. Gruschke, M. Guthoff[1], C. Hackstein, F. Hartmann, M. Heinrich, H. Held, K.H. Hoffmann, S. Honc, I. Katkov[12], J.R. Komaragiri, T. Kuhr, D. Martschei, S. Mueller, Th. Müller, M. Niegel, O. Oberst, A. Oehler, J. Ott, T. Peiffer, G. Quast, K. Rabbertz, F. Ratnikov, N. Ratnikova, M. Renz, S. Röcker, C. Saout, A. Scheurer, P. Schieferdecker, F.-P. Schilling, M. Schmanau, G. Schott, H.J. Simonis, F.M. Stober, D. Troendle, J. Wagner-Kuhr, T. Weiler, M. Zeise, E.B. Ziebarth

Institute of Nuclear Physics "Demokritos", Aghia Paraskevi, Greece
G. Daskalakis, T. Geralis, S. Kesisoglou, A. Kyriakis, D. Loukas, I. Manolakos, A. Markou, C. Markou, C. Mavrommatis, E. Ntomari, E. Petrakou

University of Athens, Athens, Greece
L. Gouskos, T.J. Mertzimekis, A. Panagiotou, N. Saoulidou, E. Stiliaris

University of Ioánnina, Ioánnina, Greece
I. Evangelou, C. Foudas[1], P. Kokkas, N. Manthos, I. Papadopoulos, V. Patras, F.A. Triantis

KFKI Research Institute for Particle and Nuclear Physics, Budapest, Hungary
A. Aranyi, G. Bencze, L. Boldizsar, C. Hajdu[1], P. Hidas, D. Horvath[14], A. Kapusi, K. Krajczar[15], F. Sikler[1], G.I. Veres[15], G. Vesztergombi[15]

Institute of Nuclear Research ATOMKI, Debrecen, Hungary
N. Beni, J. Molnar, J. Palinkas, Z. Szillasi, V. Veszpremi

University of Debrecen, Debrecen, Hungary
J. Karancsi, P. Raics, Z.L. Trocsanyi, B. Ujvari

Panjab University, Chandigarh, India
S.B. Beri, V. Bhatnagar, N. Dhingra, R. Gupta, M. Jindal, M. Kaur, J.M. Kohli, M.Z. Mehta, N. Nishu, L.K. Saini, A. Sharma, A.P. Singh, J. Singh, S.P. Singh

University of Delhi, Delhi, India
S. Ahuja, B.C. Choudhary, A. Kumar, A. Kumar, S. Malhotra, M. Naimuddin, K. Ranjan, R.K. Shivpuri

Saha Institute of Nuclear Physics, Kolkata, India
S. Banerjee, S. Bhattacharya, S. Dutta, B. Gomber, S. Jain, S. Jain, R. Khurana, S. Sarkar

Bhabha Atomic Research Centre, Mumbai, India
R.K. Choudhury, D. Dutta, S. Kailas, V. Kumar, A.K. Mohanty[1], L.M. Pant, P. Shukla

Tata Institute of Fundamental Research - EHEP, Mumbai, India
T. Aziz, M. Guchait[16], A. Gurtu[17], M. Maity[18], D. Majumder, G. Majumder, K. Mazumdar, G.B. Mohanty, B. Parida, A. Saha, K. Sudhakar, N. Wickramage

Tata Institute of Fundamental Research - HECR, Mumbai, India
S. Banerjee, S. Dugad, N.K. Mondal

Institute for Research in Fundamental Sciences (IPM), Tehran, Iran
H. Arfaei, H. Bakhshiansohi[19], S.M. Etesami[20], A. Fahim[19], M. Hashemi, H. Hesari, A. Jafari[19], M. Khakzad, A. Mohammadi[21], M. Mohammadi Najafabadi, S. Paktinat Mehdiabadi, B. Safarzadeh[22], M. Zeinali[20]

INFN Sezione di Bari [a], Università di Bari [b], Politecnico di Bari [c], Bari, Italy
M. Abbrescia[a,b], L. Barbone[a,b], C. Calabria[a,b], A. Colaleo[a], D. Creanza[a,c], N. De Filippis[a,c,1], M. De Palma[a,b], L. Fiore[a], G. Iaselli[a,c], L. Lusito[a,b], G. Maggi[a,c], M. Maggi[a], N. Manna[a,b], B. Marangelli[a,b], S. My[a,c], S. Nuzzo[a,b], N. Pacifico[a,b], A. Pompili[a,b], G. Pugliese[a,c], F. Romano[a,c], G. Selvaggi[a,b], L. Silvestris[a], S. Tupputi[a,b], G. Zito[a]

INFN Sezione di Bologna [a], Università di Bologna [b], Bologna, Italy
G. Abbiendi[a], A.C. Benvenuti[a], D. Bonacorsi[a], S. Braibant-Giacomelli[a,b], L. Brigliadori[a], P. Capiluppi[a,b], A. Castro[a,b], F.R. Cavallo[a], M. Cuffiani[a,b], G.M. Dallavalle[a], F. Fabbri[a], A. Fanfani[a,b], D. Fasanella[a,1], P. Giacomelli[a], C. Grandi[a], S. Marcellini[a], G. Masetti[a], M. Meneghelli[a,b], A. Montanari[a], F.L. Navarria[a,b], F. Odorici[a], A. Perrotta[a], F. Primavera[a], A.M. Rossi[a,b], T. Rovelli[a,b], G. Siroli[a,b], R. Travaglini[a,b]

INFN Sezione di Catania [a], Università di Catania [b], Catania, Italy
S. Albergo[a,b], G. Cappello[a,b], M. Chiorboli[a,b], S. Costa[a,b], R. Potenza[a,b], A. Tricomi[a,b], C. Tuve[a,b]

INFN Sezione di Firenze [a], Università di Firenze [b], Firenze, Italy
G. Barbagli[a], V. Ciulli[a,b], C. Civinini[a], R. D'Alessandro[a,b], E. Focardi[a,b], S. Frosali[a,b], E. Gallo[a], S. Gonzi[a,b], M. Meschini[a], S. Paoletti[a], G. Sguazzoni[a], A. Tropiano[a,1]

INFN Laboratori Nazionali di Frascati, Frascati, Italy
L. Benussi, S. Bianco, S. Colafranceschi[23], F. Fabbri, D. Piccolo

INFN Sezione di Genova, Genova, Italy
P. Fabbricatore, R. Musenich

INFN Sezione di Milano-Bicocca [a], Università di Milano-Bicocca [b], Milano, Italy
A. Benaglia[a,b,1], F. De Guio[a,b], L. Di Matteo[a,b], S. Gennai[a,1], A. Ghezzi[a,b], S. Malvezzi[a], A. Martelli[a,b], A. Massironi[a,b,1], D. Menasce[a], L. Moroni[a], M. Paganoni[a,b], D. Pedrini[a], S. Ragazzi[a,b], N. Redaelli[a], S. Sala[a], T. Tabarelli de Fatis[a,b]

INFN Sezione di Napoli [a], Università di Napoli "Federico II" [b], Napoli, Italy
S. Buontempo[a], C.A. Carrillo Montoya[a,1], N. Cavallo[a,24], A. De Cosa[a,b], O. Dogangun[a,b], F. Fabozzi[a,24], A.O.M. Iorio[a,1], L. Lista[a], M. Merola[a,b], P. Paolucci[a]

INFN Sezione di Padova [a], Università di Padova [b], Università di Trento (Trento) [c], Padova, Italy
P. Azzi[a], N. Bacchetta[a,1], P. Bellan[a,b], M. Biasotto[a,25], D. Bisello[a,b], A. Branca[a], R. Carlin[a,b], P. Checchia[a], T. Dorigo[a], U. Dosselli[a], F. Gasparini[a,b], A. Gozzelino[a], M. Gulmini[a,25], S. Lacaprara[a,25], I. Lazzizzera[a,c], M. Margoni[a,b], G. Maron[a,25], A.T. Meneguzzo[a,b], M. Nespolo[a,1], L. Perrozzi[a], N. Pozzobon[a,b], P. Ronchese[a,b], F. Simonetto[a,b], E. Torassa[a], M. Tosi[a,b,1], A. Triossi[a], S. Vanini[a,b], P. Zotto[a,b]

INFN Sezione di Pavia [a], Università di Pavia [b], Pavia, Italy
P. Baesso[a,b], U. Berzano[a], S.P. Ratti[a,b], C. Riccardi[a,b], P. Torre[a,b], P. Vitulo[a,b], C. Viviani[a,b]

INFN Sezione di Perugia [a], Università di Perugia [b], Perugia, Italy
M. Biasini[a,b], G.M. Bilei[a], B. Caponeri[a,b], L. Fanò[a,b], P. Lariccia[a,b], A. Lucaroni[a,b,1], G. Mantovani[a,b], M. Menichelli[a], A. Nappi[a,b], F. Romeo[a,b], A. Santocchia[a,b], S. Taroni[a,b,1], M. Valdata[a,b]

INFN Sezione di Pisa [a], Università di Pisa [b], Scuola Normale Superiore di Pisa [c], Pisa, Italy
P. Azzurri[a,c], G. Bagliesi[a], T. Boccali[a], G. Broccolo[a,c], R. Castaldi[a], R.T. D'Agnolo[a,c], R. Dell'Orso[a], F. Fiori[a,b], L. Foà[a,c], A. Giassi[a], A. Kraan[a], F. Ligabue[a,c], T. Lomtadze[a],

L. Martini[a,26], A. Messineo[a,b], F. Palla[a], F. Palmonari[a], A. Rizzi, G. Segneri[a], A.T. Serban[a], P. Spagnolo[a], R. Tenchini[a], G. Tonelli[a,b,1], A. Venturi[a,1], P.G. Verdini[a]

INFN Sezione di Roma [a], Università di Roma "La Sapienza" [b], Roma, Italy
L. Barone[a,b], F. Cavallari[a], D. Del Re[a,b,1], M. Diemoz[a], D. Franci[a,b], M. Grassi[a,1], E. Longo[a,b], P. Meridiani[a], S. Nourbakhsh[a], G. Organtini[a,b], F. Pandolfi[a,b], R. Paramatti[a], S. Rahatlou[a,b], M. Sigamani[a]

INFN Sezione di Torino [a], Università di Torino [b], Università del Piemonte Orientale (Novara) [c], Torino, Italy
N. Amapane[a,b], R. Arcidiacono[a,c], S. Argiro[a,b], M. Arneodo[a,c], C. Biino[a], C. Botta[a,b], N. Cartiglia[a], R. Castello[a,b], M. Costa[a,b], N. Demaria[a], A. Graziano[a,b], C. Mariotti[a], S. Maselli[a], E. Migliore[a,b], V. Monaco[a,b], M. Musich[a], M.M. Obertino[a,c], N. Pastrone[a], M. Pelliccioni[a], A. Potenza[a,b], A. Romero[a,b], M. Ruspa[a,c], R. Sacchi[a,b], V. Sola[a,b], A. Solano[a,b], A. Staiano[a], A. Vilela Pereira[a]

INFN Sezione di Trieste [a], Università di Trieste [b], Trieste, Italy
S. Belforte[a], F. Cossutti[a], G. Della Ricca[a,b], B. Gobbo[a], M. Marone[a,b], D. Montanino[a,b,1], A. Penzo[a]

Kangwon National University, Chunchon, Korea
S.G. Heo, S.K. Nam

Kyungpook National University, Daegu, Korea
S. Chang, J. Chung, D.H. Kim, G.N. Kim, J.E. Kim, D.J. Kong, H. Park, S.R. Ro, D.C. Son, T. Son

Chonnam National University, Institute for Universe and Elementary Particles, Kwangju, Korea
J.Y. Kim, Zero J. Kim, S. Song

Konkuk University, Seoul, Korea
H.Y. Jo

Korea University, Seoul, Korea
S. Choi, D. Gyun, B. Hong, M. Jo, H. Kim, T.J. Kim, K.S. Lee, D.H. Moon, S.K. Park, E. Seo, K.S. Sim

University of Seoul, Seoul, Korea
M. Choi, S. Kang, H. Kim, J.H. Kim, C. Park, I.C. Park, S. Park, G. Ryu

Sungkyunkwan University, Suwon, Korea
Y. Cho, Y. Choi, Y.K. Choi, J. Goh, M.S. Kim, B. Lee, J. Lee, S. Lee, H. Seo, I. Yu

Vilnius University, Vilnius, Lithuania
M.J. Bilinskas, I. Grigelionis, M. Janulis, D. Martisiute, P. Petrov, M. Polujanskas, T. Sabonis

Centro de Investigacion y de Estudios Avanzados del IPN, Mexico City, Mexico
H. Castilla-Valdez, E. De La Cruz-Burelo, I. Heredia-de La Cruz, R. Lopez-Fernandez, R. Magaña Villalba, J. Martínez-Ortega, A. Sánchez-Hernández, L.M. Villasenor-Cendejas

Universidad Iberoamericana, Mexico City, Mexico
S. Carrillo Moreno, F. Vazquez Valencia

Benemerita Universidad Autonoma de Puebla, Puebla, Mexico
H.A. Salazar Ibarguen

Universidad Autónoma de San Luis Potosí, San Luis Potosí, Mexico
E. Casimiro Linares, A. Morelos Pineda, M.A. Reyes-Santos

University of Auckland, Auckland, New Zealand
D. Krofcheck, J. Tam

University of Canterbury, Christchurch, New Zealand
A.J. Bell, P.H. Butler, R. Doesburg, S. Reucroft, H. Silverwood

National Centre for Physics, Quaid-I-Azam University, Islamabad, Pakistan
M. Ahmad, M.I. Asghar, H.R. Hoorani, S. Khalid, W.A. Khan, T. Khurshid, S. Qazi, M.A. Shah, M. Shoaib

Institute of Experimental Physics, Faculty of Physics, University of Warsaw, Warsaw, Poland
G. Brona, M. Cwiok, W. Dominik, K. Doroba, A. Kalinowski, M. Konecki, J. Krolikowski

Soltan Institute for Nuclear Studies, Warsaw, Poland
H. Bialkowska, B. Boimska, T. Frueboes, R. Gokieli, M. Górski, M. Kazana, K. Nawrocki, K. Romanowska-Rybinska, M. Szleper, G. Wrochna, P. Zalewski

Laboratório de Instrumentação e Física Experimental de Partículas, Lisboa, Portugal
N. Almeida, P. Bargassa, A. David, P. Faccioli, P.G. Ferreira Parracho, M. Gallinaro, P. Musella, A. Nayak, J. Pela[1], P.Q. Ribeiro, J. Seixas, J. Varela

Joint Institute for Nuclear Research, Dubna, Russia
S. Afanasiev, I. Belotelov, P. Bunin, M. Gavrilenko, I. Golutvin, I. Gorbunov, A. Kamenev, V. Karjavin, G. Kozlov, A. Lanev, P. Moisenz, V. Palichik, V. Perelygin, S. Shmatov, V. Smirnov, A. Volodko, A. Zarubin

Petersburg Nuclear Physics Institute, Gatchina (St Petersburg), Russia
S. Evstyukhin, V. Golovtsov, Y. Ivanov, V. Kim, P. Levchenko, V. Murzin, V. Oreshkin, I. Smirnov, V. Sulimov, L. Uvarov, S. Vavilov, A. Vorobyev, An. Vorobyev

Institute for Nuclear Research, Moscow, Russia
Yu. Andreev, A. Dermenev, S. Gninenko, N. Golubev, M. Kirsanov, N. Krasnikov, V. Matveev, A. Pashenkov, A. Toropin, S. Troitsky

Institute for Theoretical and Experimental Physics, Moscow, Russia
V. Epshteyn, M. Erofeeva, V. Gavrilov, M. Kossov[1], A. Krokhotin, N. Lychkovskaya, V. Popov, G. Safronov, S. Semenov, V. Stolin, E. Vlasov, A. Zhokin

Moscow State University, Moscow, Russia
A. Belyaev, E. Boos, A. Ershov, A. Gribushin, O. Kodolova, V. Korotkikh, I. Lokhtin, A. Markina, S. Obraztsov, M. Perfilov, S. Petrushanko, L. Sarycheva, V. Savrin, A. Snigirev, I. Vardanyan

P.N. Lebedev Physical Institute, Moscow, Russia
V. Andreev, M. Azarkin, I. Dremin, M. Kirakosyan, A. Leonidov, G. Mesyats, S.V. Rusakov, A. Vinogradov

State Research Center of Russian Federation, Institute for High Energy Physics, Protvino, Russia
I. Azhgirey, I. Bayshev, S. Bitioukov, V. Grishin[1], V. Kachanov, D. Konstantinov, A. Korablev, V. Krychkine, V. Petrov, R. Ryutin, A. Sobol, L. Tourtchanovitch, S. Troshin, N. Tyurin, A. Uzunian, A. Volkov

University of Belgrade, Faculty of Physics and Vinca Institute of Nuclear Sciences, Belgrade, Serbia
P. Adzic[27], M. Djordjevic, M. Ekmedzic, D. Krpic[27], J. Milosevic

Centro de Investigaciones Energéticas Medioambientales y Tecnológicas (CIEMAT), Madrid, Spain
M. Aguilar-Benitez, J. Alcaraz Maestre, P. Arce, C. Battilana, E. Calvo, M. Cerrada, M. Chamizo Llatas, N. Colino, B. De La Cruz, A. Delgado Peris, C. Diez Pardos, D. Domínguez Vázquez, C. Fernandez Bedoya, J.P. Fernández Ramos, A. Ferrando, J. Flix, M.C. Fouz, P. Garcia-Abia, O. Gonzalez Lopez, S. Goy Lopez, J.M. Hernandez, M.I. Josa, G. Merino, J. Puerta Pelayo, I. Redondo, L. Romero, J. Santaolalla, M.S. Soares, C. Willmott

Universidad Autónoma de Madrid, Madrid, Spain
C. Albajar, G. Codispoti, J.F. de Trocóniz

Universidad de Oviedo, Oviedo, Spain
J. Cuevas, J. Fernandez Menendez, S. Folgueras, I. Gonzalez Caballero, L. Lloret Iglesias, J.M. Vizan Garcia

Instituto de Física de Cantabria (IFCA), CSIC-Universidad de Cantabria, Santander, Spain
J.A. Brochero Cifuentes, I.J. Cabrillo, A. Calderon, S.H. Chuang, J. Duarte Campderros, M. Felcini[28], M. Fernandez, G. Gomez, J. Gonzalez Sanchez, C. Jorda, P. Lobelle Pardo, A. Lopez Virto, J. Marco, R. Marco, C. Martinez Rivero, F. Matorras, F.J. Munoz Sanchez, J. Piedra Gomez[29], T. Rodrigo, A.Y. Rodríguez-Marrero, A. Ruiz-Jimeno, L. Scodellaro, M. Sobron Sanudo, I. Vila, R. Vilar Cortabitarte

CERN, European Organization for Nuclear Research, Geneva, Switzerland
D. Abbaneo, E. Auffray, G. Auzinger, P. Baillon, A.H. Ball, D. Barney, C. Bernet[5], W. Bialas, P. Bloch, A. Bocci, H. Breuker, K. Bunkowski, T. Camporesi, G. Cerminara, T. Christiansen, J.A. Coarasa Perez, B. Curé, D. D'Enterria, A. De Roeck, S. Di Guida, M. Dobson, N. Dupont-Sagorin, A. Elliott-Peisert, B. Frisch, W. Funk, A. Gaddi, G. Georgiou, H. Gerwig, M. Giffels, D. Gigi, K. Gill, D. Giordano, M. Giunta, F. Glege, R. Gomez-Reino Garrido, M. Gouzevitch, P. Govoni, S. Gowdy, R. Guida, L. Guiducci, S. Gundacker, M. Hansen, C. Hartl, J. Harvey, J. Hegeman, B. Hegner, H.F. Hoffmann, V. Innocente, P. Janot, K. Kaadze, E. Karavakis, P. Lecoq, P. Lenzi, C. Lourenço, T. Mäki, M. Malberti, L. Malgeri, M. Mannelli, L. Masetti, G. Mavromanolakis, F. Meijers, S. Mersi, E. Meschi, R. Moser, M.U. Mozer, M. Mulders, E. Nesvold, M. Nguyen, T. Orimoto, L. Orsini, E. Palencia Cortezon, E. Perez, A. Petrilli, A. Pfeiffer, M. Pierini, M. Pimiä, D. Piparo, G. Polese, L. Quertenmont, A. Racz, W. Reece, J. Rodrigues Antunes, G. Rolandi[30], T. Rommerskirchen, C. Rovelli[31], M. Rovere, H. Sakulin, F. Santanastasio, C. Schäfer, C. Schwick, I. Segoni, A. Sharma, P. Siegrist, P. Silva, M. Simon, P. Sphicas[32], D. Spiga, M. Spiropulu[4], M. Stoye, A. Tsirou, P. Vichoudis, H.K. Wöhri, S.D. Worm[33], W.D. Zeuner

Paul Scherrer Institut, Villigen, Switzerland
W. Bertl, K. Deiters, W. Erdmann, K. Gabathuler, R. Horisberger, Q. Ingram, H.C. Kaestli, S. König, D. Kotlinski, U. Langenegger, F. Meier, D. Renker, T. Rohe, J. Sibille[34]

Institute for Particle Physics, ETH Zurich, Zurich, Switzerland
L. Bäni, P. Bortignon, B. Casal, N. Chanon, Z. Chen, S. Cittolin, A. Deisher, G. Dissertori, M. Dittmar, J. Eugster, K. Freudenreich, C. Grab, P. Lecomte, W. Lustermann, C. Marchica[35], P. Martinez Ruiz del Arbol, P. Milenovic[36], N. Mohr, F. Moortgat, C. Nägeli[35], P. Nef, F. Nessi-Tedaldi, L. Pape, F. Pauss, M. Peruzzi, F.J. Ronga, M. Rossini, L. Sala, A.K. Sanchez, M.-

C. Sawley, A. Starodumov[37], B. Stieger, M. Takahashi, L. Tauscher[†], A. Thea, K. Theofilatos, D. Treille, C. Urscheler, R. Wallny, H.A. Weber, L. Wehrli, J. Weng

Universität Zürich, Zurich, Switzerland
E. Aguilo, C. Amsler, V. Chiochia, S. De Visscher, C. Favaro, M. Ivova Rikova, B. Millan Mejias, P. Otiougova, P. Robmann, A. Schmidt, H. Snoek, M. Verzetti

National Central University, Chung-Li, Taiwan
Y.H. Chang, K.H. Chen, C.M. Kuo, S.W. Li, W. Lin, Z.K. Liu, Y.J. Lu, D. Mekterovic, R. Volpe, S.S. Yu

National Taiwan University (NTU), Taipei, Taiwan
P. Bartalini, P. Chang, Y.H. Chang, Y.W. Chang, Y. Chao, K.F. Chen, C. Dietz, U. Grundler, W.-S. Hou, Y. Hsiung, K.Y. Kao, Y.J. Lei, R.-S. Lu, J.G. Shiu, Y.M. Tzeng, X. Wan, M. Wang

Cukurova University, Adana, Turkey
A. Adiguzel, M.N. Bakirci[38], S. Cerci[39], C. Dozen, I. Dumanoglu, E. Eskut, S. Girgis, G. Gokbulut, I. Hos, E.E. Kangal, G. Karapinar, A. Kayis Topaksu, G. Onengut, K. Ozdemir, S. Ozturk[40], A. Polatoz, K. Sogut[41], D. Sunar Cerci[39], B. Tali[39], H. Topakli[38], D. Uzun, L.N. Vergili, M. Vergili

Middle East Technical University, Physics Department, Ankara, Turkey
I.V. Akin, T. Aliev, B. Bilin, S. Bilmis, M. Deniz, H. Gamsizkan, A.M. Guler, K. Ocalan, A. Ozpineci, M. Serin, R. Sever, U.E. Surat, M. Yalvac, E. Yildirim, M. Zeyrek

Bogazici University, Istanbul, Turkey
M. Deliomeroglu, E. Gülmez, B. Isildak, M. Kaya[42], O. Kaya[42], M. Özbek, S. Ozkorucuklu[43], N. Sonmez[44]

National Scientific Center, Kharkov Institute of Physics and Technology, Kharkov, Ukraine
L. Levchuk

University of Bristol, Bristol, United Kingdom
F. Bostock, J.J. Brooke, E. Clement, D. Cussans, R. Frazier, J. Goldstein, M. Grimes, G.P. Heath, H.F. Heath, L. Kreczko, S. Metson, D.M. Newbold[33], K. Nirunpong, A. Poll, S. Senkin, V.J. Smith, T. Williams

Rutherford Appleton Laboratory, Didcot, United Kingdom
L. Basso[45], A. Belyaev[45], C. Brew, R.M. Brown, B. Camanzi, D.J.A. Cockerill, J.A. Coughlan, K. Harder, S. Harper, J. Jackson, B.W. Kennedy, E. Olaiya, D. Petyt, B.C. Radburn-Smith, C.H. Shepherd-Themistocleous, I.R. Tomalin, W.J. Womersley

Imperial College, London, United Kingdom
R. Bainbridge, G. Ball, R. Beuselinck, O. Buchmuller, D. Colling, N. Cripps, M. Cutajar, P. Dauncey, G. Davies, M. Della Negra, W. Ferguson, J. Fulcher, D. Futyan, A. Gilbert, A. Guneratne Bryer, G. Hall, Z. Hatherell, J. Hays, G. Iles, M. Jarvis, G. Karapostoli, L. Lyons, A.-M. Magnan, J. Marrouche, B. Mathias, R. Nandi, J. Nash, A. Nikitenko[37], A. Papageorgiou, M. Pesaresi, K. Petridis, M. Pioppi[46], D.M. Raymond, S. Rogerson, N. Rompotis, A. Rose, M.J. Ryan, C. Seez, P. Sharp, A. Sparrow, A. Tapper, S. Tourneur, M. Vazquez Acosta, T. Virdee, S. Wakefield, N. Wardle, D. Wardrope, T. Whyntie

Brunel University, Uxbridge, United Kingdom
M. Barrett, M. Chadwick, J.E. Cole, P.R. Hobson, A. Khan, P. Kyberd, D. Leslie, W. Martin, I.D. Reid, L. Teodorescu, M. Turner

Baylor University, Waco, USA
K. Hatakeyama, H. Liu, T. Scarborough

The University of Alabama, Tuscaloosa, USA
C. Henderson

Boston University, Boston, USA
A. Avetisyan, T. Bose, E. Carrera Jarrin, C. Fantasia, A. Heister, J. St. John, P. Lawson, D. Lazic, J. Rohlf, D. Sperka, L. Sulak

Brown University, Providence, USA
S. Bhattacharya, D. Cutts, A. Ferapontov, U. Heintz, S. Jabeen, G. Kukartsev, G. Landsberg, M. Luk, M. Narain, D. Nguyen, M. Segala, T. Sinthuprasith, T. Speer, K.V. Tsang

University of California, Davis, Davis, USA
R. Breedon, G. Breto, M. Calderon De La Barca Sanchez, S. Chauhan, M. Chertok, J. Conway, R. Conway, P.T. Cox, J. Dolen, R. Erbacher, R. Houtz, W. Ko, A. Kopecky, R. Lander, O. Mall, T. Miceli, D. Pellett, J. Robles, B. Rutherford, M. Searle, J. Smith, M. Squires, M. Tripathi, R. Vasquez Sierra

University of California, Los Angeles, Los Angeles, USA
V. Andreev, K. Arisaka, D. Cline, R. Cousins, J. Duris, S. Erhan, P. Everaerts, C. Farrell, J. Hauser, M. Ignatenko, C. Jarvis, C. Plager, G. Rakness, P. Schlein†, J. Tucker, V. Valuev, M. Weber

University of California, Riverside, Riverside, USA
J. Babb, R. Clare, J. Ellison, J.W. Gary, F. Giordano, G. Hanson, G.Y. Jeng, S.C. Kao, H. Liu, O.R. Long, A. Luthra, H. Nguyen, S. Paramesvaran, J. Sturdy, S. Sumowidagdo, R. Wilken, S. Wimpenny

University of California, San Diego, La Jolla, USA
W. Andrews, J.G. Branson, G.B. Cerati, D. Evans, F. Golf, A. Holzner, R. Kelley, M. Lebourgeois, J. Letts, I. Macneill, B. Mangano, S. Padhi, C. Palmer, G. Petrucciani, H. Pi, M. Pieri, R. Ranieri, M. Sani, I. Sfiligoi, V. Sharma, S. Simon, E. Sudano, M. Tadel, Y. Tu, A. Vartak, S. Wasserbaech[47], F. Würthwein, A. Yagil, J. Yoo

University of California, Santa Barbara, Santa Barbara, USA
D. Barge, R. Bellan, C. Campagnari, M. D'Alfonso, T. Danielson, K. Flowers, P. Geffert, C. George, J. Incandela, C. Justus, P. Kalavase, S.A. Koay, D. Kovalskyi[1], V. Krutelyov, S. Lowette, N. Mccoll, S.D. Mullin, V. Pavlunin, F. Rebassoo, J. Ribnik, J. Richman, R. Rossin, D. Stuart, W. To, J.R. Vlimant, C. West

California Institute of Technology, Pasadena, USA
A. Apresyan, A. Bornheim, J. Bunn, Y. Chen, E. Di Marco, J. Duarte, M. Gataullin, Y. Ma, A. Mott, H.B. Newman, C. Rogan, V. Timciuc, P. Traczyk, J. Veverka, R. Wilkinson, Y. Yang, R.Y. Zhu

Carnegie Mellon University, Pittsburgh, USA
B. Akgun, R. Carroll, T. Ferguson, Y. Iiyama, D.W. Jang, S.Y. Jun, Y.F. Liu, M. Paulini, J. Russ, H. Vogel, I. Vorobiev

University of Colorado at Boulder, Boulder, USA
J.P. Cumalat, M.E. Dinardo, B.R. Drell, C.J. Edelmaier, W.T. Ford, A. Gaz, B. Heyburn, E. Luiggi Lopez, U. Nauenberg, J.G. Smith, K. Stenson, K.A. Ulmer, S.R. Wagner, S.L. Zang

Cornell University, Ithaca, USA
L. Agostino, J. Alexander, A. Chatterjee, N. Eggert, L.K. Gibbons, B. Heltsley, W. Hopkins, A. Khukhunaishvili, B. Kreis, G. Nicolas Kaufman, J.R. Patterson, D. Puigh, A. Ryd, E. Salvati, X. Shi, W. Sun, W.D. Teo, J. Thom, J. Thompson, J. Vaughan, Y. Weng, L. Winstrom, P. Wittich

Fairfield University, Fairfield, USA
A. Biselli, G. Cirino, D. Winn

Fermi National Accelerator Laboratory, Batavia, USA
S. Abdullin, M. Albrow, J. Anderson, G. Apollinari, M. Atac, J.A. Bakken, L.A.T. Bauerdick, A. Beretvas, J. Berryhill, P.C. Bhat, I. Bloch, K. Burkett, J.N. Butler, V. Chetluru, H.W.K. Cheung, F. Chlebana, S. Cihangir, W. Cooper, D.P. Eartly, V.D. Elvira, S. Esen, I. Fisk, J. Freeman, Y. Gao, E. Gottschalk, D. Green, O. Gutsche, J. Hanlon, R.M. Harris, J. Hirschauer, B. Hooberman, H. Jensen, S. Jindariani, M. Johnson, U. Joshi, B. Klima, K. Kousouris, S. Kunori, S. Kwan, C. Leonidopoulos, D. Lincoln, R. Lipton, J. Lykken, K. Maeshima, J.M. Marraffino, S. Maruyama, D. Mason, P. McBride, T. Miao, K. Mishra, S. Mrenna, Y. Musienko[48], C. Newman-Holmes, V. O'Dell, J. Pivarski, R. Pordes, O. Prokofyev, T. Schwarz, E. Sexton-Kennedy, S. Sharma, W.J. Spalding, L. Spiegel, P. Tan, L. Taylor, S. Tkaczyk, L. Uplegger, E.W. Vaandering, R. Vidal, J. Whitmore, W. Wu, F. Yang, F. Yumiceva, J.C. Yun

University of Florida, Gainesville, USA
D. Acosta, P. Avery, D. Bourilkov, M. Chen, S. Das, M. De Gruttola, G.P. Di Giovanni, D. Dobur, A. Drozdetskiy, R.D. Field, M. Fisher, Y. Fu, I.K. Furic, J. Gartner, S. Goldberg, J. Hugon, B. Kim, J. Konigsberg, A. Korytov, A. Kropivnitskaya, T. Kypreos, J.F. Low, K. Matchev, G. Mitselmakher, L. Muniz, M. Park, R. Remington, A. Rinkevicius, M. Schmitt, B. Scurlock, P. Sellers, N. Skhirtladze, M. Snowball, D. Wang, J. Yelton, M. Zakaria

Florida International University, Miami, USA
V. Gaultney, L.M. Lebolo, S. Linn, P. Markowitz, G. Martinez, J.L. Rodriguez

Florida State University, Tallahassee, USA
T. Adams, A. Askew, J. Bochenek, J. Chen, B. Diamond, S.V. Gleyzer, J. Haas, S. Hagopian, V. Hagopian, M. Jenkins, K.F. Johnson, H. Prosper, S. Sekmen, V. Veeraraghavan

Florida Institute of Technology, Melbourne, USA
M.M. Baarmand, B. Dorney, M. Hohlmann, H. Kalakhety, I. Vodopiyanov

University of Illinois at Chicago (UIC), Chicago, USA
M.R. Adams, I.M. Anghel, L. Apanasevich, Y. Bai, V.E. Bazterra, R.R. Betts, J. Callner, R. Cavanaugh, C. Dragoiu, L. Gauthier, C.E. Gerber, D.J. Hofman, S. Khalatyan, G.J. Kunde[49], F. Lacroix, M. Malek, C. O'Brien, C. Silkworth, C. Silvestre, D. Strom, N. Varelas

The University of Iowa, Iowa City, USA
U. Akgun, E.A. Albayrak, B. Bilki, W. Clarida, F. Duru, S. Griffiths, C.K. Lae, E. McCliment, J.-P. Merlo, H. Mermerkaya[50], A. Mestvirishvili, A. Moeller, J. Nachtman, C.R. Newsom, E. Norbeck, J. Olson, Y. Onel, F. Ozok, S. Sen, E. Tiras, J. Wetzel, T. Yetkin, K. Yi

Johns Hopkins University, Baltimore, USA
B.A. Barnett, B. Blumenfeld, S. Bolognesi, A. Bonato, C. Eskew, D. Fehling, G. Giurgiu, A.V. Gritsan, Z.J. Guo, G. Hu, P. Maksimovic, S. Rappoccio, M. Swartz, N.V. Tran, A. Whitbeck

The University of Kansas, Lawrence, USA
P. Baringer, A. Bean, G. Benelli, O. Grachov, R.P. Kenny Iii, M. Murray, D. Noonan, S. Sanders, R. Stringer, G. Tinti, J.S. Wood, V. Zhukova

Kansas State University, Manhattan, USA
A.F. Barfuss, T. Bolton, I. Chakaberia, A. Ivanov, S. Khalil, M. Makouski, Y. Maravin, S. Shrestha, I. Svintradze

Lawrence Livermore National Laboratory, Livermore, USA
J. Gronberg, D. Lange, D. Wright

University of Maryland, College Park, USA
A. Baden, M. Boutemeur, B. Calvert, S.C. Eno, J.A. Gomez, N.J. Hadley, R.G. Kellogg, M. Kirn, Y. Lu, A.C. Mignerey, A. Peterman, K. Rossato, P. Rumerio, A. Skuja, J. Temple, M.B. Tonjes, S.C. Tonwar, E. Twedt

Massachusetts Institute of Technology, Cambridge, USA
B. Alver, G. Bauer, J. Bendavid, W. Busza, E. Butz, I.A. Cali, M. Chan, V. Dutta, G. Gomez Ceballos, M. Goncharov, K.A. Hahn, P. Harris, Y. Kim, M. Klute, Y.-J. Lee, W. Li, P.D. Luckey, T. Ma, S. Nahn, C. Paus, D. Ralph, C. Roland, G. Roland, M. Rudolph, G.S.F. Stephans, F. Stöckli, K. Sumorok, K. Sung, D. Velicanu, E.A. Wenger, R. Wolf, B. Wyslouch, S. Xie, M. Yang, Y. Yilmaz, A.S. Yoon, M. Zanetti

University of Minnesota, Minneapolis, USA
S.I. Cooper, P. Cushman, B. Dahmes, A. De Benedetti, G. Franzoni, A. Gude, J. Haupt, K. Klapoetke, Y. Kubota, J. Mans, N. Pastika, V. Rekovic, R. Rusack, M. Sasseville, A. Singovsky, N. Tambe, J. Turkewitz

University of Mississippi, University, USA
L.M. Cremaldi, R. Godang, R. Kroeger, L. Perera, R. Rahmat, D.A. Sanders, D. Summers

University of Nebraska-Lincoln, Lincoln, USA
E. Avdeeva, K. Bloom, S. Bose, J. Butt, D.R. Claes, A. Dominguez, M. Eads, P. Jindal, J. Keller, I. Kravchenko, J. Lazo-Flores, H. Malbouisson, S. Malik, G.R. Snow

State University of New York at Buffalo, Buffalo, USA
U. Baur, A. Godshalk, I. Iashvili, S. Jain, A. Kharchilava, A. Kumar, K. Smith, Z. Wan

Northeastern University, Boston, USA
G. Alverson, E. Barberis, D. Baumgartel, M. Chasco, D. Trocino, D. Wood, J. Zhang

Northwestern University, Evanston, USA
A. Anastassov, A. Kubik, N. Mucia, N. Odell, R.A. Ofierzynski, B. Pollack, A. Pozdnyakov, M. Schmitt, S. Stoynev, M. Velasco, S. Won

University of Notre Dame, Notre Dame, USA
L. Antonelli, D. Berry, A. Brinkerhoff, M. Hildreth, C. Jessop, D.J. Karmgard, J. Kolb, T. Kolberg, K. Lannon, W. Luo, S. Lynch, N. Marinelli, D.M. Morse, T. Pearson, R. Ruchti, J. Slaunwhite, N. Valls, M. Wayne, J. Ziegler

The Ohio State University, Columbus, USA
B. Bylsma, L.S. Durkin, C. Hill, P. Killewald, K. Kotov, T.Y. Ling, M. Rodenburg, C. Vuosalo, G. Williams

Princeton University, Princeton, USA
N. Adam, E. Berry, P. Elmer, D. Gerbaudo, V. Halyo, P. Hebda, A. Hunt, E. Laird, D. Lopes Pegna, P. Lujan, D. Marlow, T. Medvedeva, M. Mooney, J. Olsen, P. Piroué, X. Quan, A. Raval, H. Saka, D. Stickland, C. Tully, J.S. Werner, A. Zuranski

University of Puerto Rico, Mayaguez, USA
J.G. Acosta, X.T. Huang, A. Lopez, H. Mendez, S. Oliveros, J.E. Ramirez Vargas, A. Zatserklyaniy

Purdue University, West Lafayette, USA
E. Alagoz, V.E. Barnes, D. Benedetti, G. Bolla, L. Borrello, D. Bortoletto, M. De Mattia, A. Everett, L. Gutay, Z. Hu, M. Jones, O. Koybasi, M. Kress, A.T. Laasanen, N. Leonardo, V. Maroussov, P. Merkel, D.H. Miller, N. Neumeister, I. Shipsey, D. Silvers, A. Svyatkovskiy, M. Vidal Marono, H.D. Yoo, J. Zablocki, Y. Zheng

Purdue University Calumet, Hammond, USA
S. Guragain, N. Parashar

Rice University, Houston, USA
A. Adair, C. Boulahouache, V. Cuplov, K.M. Ecklund, F.J.M. Geurts, B.P. Padley, R. Redjimi, J. Roberts, J. Zabel

University of Rochester, Rochester, USA
B. Betchart, A. Bodek, Y.S. Chung, R. Covarelli, P. de Barbaro, R. Demina, Y. Eshaq, H. Flacher, A. Garcia-Bellido, P. Goldenzweig, Y. Gotra, J. Han, A. Harel, D.C. Miner, G. Petrillo, W. Sakumoto, D. Vishnevskiy, M. Zielinski

The Rockefeller University, New York, USA
A. Bhatti, R. Ciesielski, L. Demortier, K. Goulianos, G. Lungu, S. Malik, C. Mesropian

Rutgers, the State University of New Jersey, Piscataway, USA
S. Arora, O. Atramentov, A. Barker, J.P. Chou, C. Contreras-Campana, E. Contreras-Campana, D. Duggan, D. Ferencek, Y. Gershtein, R. Gray, E. Halkiadakis, D. Hidas, D. Hits, A. Lath, S. Panwalkar, M. Park, R. Patel, A. Richards, K. Rose, S. Salur, S. Schnetzer, S. Somalwar, R. Stone, S. Thomas

University of Tennessee, Knoxville, USA
G. Cerizza, M. Hollingsworth, S. Spanier, Z.C. Yang, A. York

Texas A&M University, College Station, USA
R. Eusebi, W. Flanagan, J. Gilmore, T. Kamon[51], V. Khotilovich, R. Montalvo, I. Osipenkov, Y. Pakhotin, A. Perloff, J. Roe, A. Safonov, S. Sengupta, I. Suarez, A. Tatarinov, D. Toback

Texas Tech University, Lubbock, USA
N. Akchurin, C. Bardak, J. Damgov, P.R. Dudero, C. Jeong, K. Kovitanggoon, S.W. Lee, T. Libeiro, P. Mane, Y. Roh, A. Sill, I. Volobouev, R. Wigmans, E. Yazgan

Vanderbilt University, Nashville, USA
E. Appelt, E. Brownson, D. Engh, C. Florez, W. Gabella, A. Gurrola, M. Issah, W. Johns, C. Johnston, P. Kurt, C. Maguire, A. Melo, P. Sheldon, B. Snook, S. Tuo, J. Velkovska

University of Virginia, Charlottesville, USA
M.W. Arenton, M. Balazs, S. Boutle, S. Conetti, B. Cox, B. Francis, S. Goadhouse, J. Goodell, R. Hirosky, A. Ledovskoy, C. Lin, C. Neu, J. Wood, R. Yohay

Wayne State University, Detroit, USA
S. Gollapinni, R. Harr, P.E. Karchin, C. Kottachchi Kankanamge Don, P. Lamichhane, M. Mattson, C. Milstène, A. Sakharov

University of Wisconsin, Madison, USA
M. Anderson, M. Bachtis, D. Belknap, J.N. Bellinger, J. Bernardini, D. Carlsmith, M. Cepeda,

S. Dasu, J. Efron, E. Friis, L. Gray, K.S. Grogg, M. Grothe, R. Hall-Wilton, M. Herndon, A. Hervé, P. Klabbers, J. Klukas, A. Lanaro, C. Lazaridis, J. Leonard, R. Loveless, A. Mohapatra, I. Ojalvo, G.A. Pierro, I. Ross, A. Savin, W.H. Smith, J. Swanson, M. Weinberg

†: Deceased
1: Also at CERN, European Organization for Nuclear Research, Geneva, Switzerland
2: Also at National Institute of Chemical Physics and Biophysics, Tallinn, Estonia
3: Also at Universidade Federal do ABC, Santo Andre, Brazil
4: Also at California Institute of Technology, Pasadena, USA
5: Also at Laboratoire Leprince-Ringuet, Ecole Polytechnique, IN2P3-CNRS, Palaiseau, France
6: Also at Suez Canal University, Suez, Egypt
7: Also at Cairo University, Cairo, Egypt
8: Also at British University, Cairo, Egypt
9: Also at Fayoum University, El-Fayoum, Egypt
10: Also at Soltan Institute for Nuclear Studies, Warsaw, Poland
11: Also at Université de Haute-Alsace, Mulhouse, France
12: Also at Moscow State University, Moscow, Russia
13: Also at Brandenburg University of Technology, Cottbus, Germany
14: Also at Institute of Nuclear Research ATOMKI, Debrecen, Hungary
15: Also at Eötvös Loránd University, Budapest, Hungary
16: Also at Tata Institute of Fundamental Research - HECR, Mumbai, India
17: Now at King Abdulaziz University, Jeddah, Saudi Arabia
18: Also at University of Visva-Bharati, Santiniketan, India
19: Also at Sharif University of Technology, Tehran, Iran
20: Also at Isfahan University of Technology, Isfahan, Iran
21: Also at Shiraz University, Shiraz, Iran
22: Also at Plasma Physics Research Center, Science and Research Branch, Islamic Azad University, Teheran, Iran
23: Also at Facoltà Ingegneria Università di Roma, Roma, Italy
24: Also at Università della Basilicata, Potenza, Italy
25: Also at Laboratori Nazionali di Legnaro dell' INFN, Legnaro, Italy
26: Also at Università degli studi di Siena, Siena, Italy
27: Also at Faculty of Physics of University of Belgrade, Belgrade, Serbia
28: Also at University of California, Los Angeles, Los Angeles, USA
29: Also at University of Florida, Gainesville, USA
30: Also at Scuola Normale e Sezione dell' INFN, Pisa, Italy
31: Also at INFN Sezione di Roma; Università di Roma "La Sapienza", Roma, Italy
32: Also at University of Athens, Athens, Greece
33: Also at Rutherford Appleton Laboratory, Didcot, United Kingdom
34: Also at The University of Kansas, Lawrence, USA
35: Also at Paul Scherrer Institut, Villigen, Switzerland
36: Also at University of Belgrade, Faculty of Physics and Vinca Institute of Nuclear Sciences, Belgrade, Serbia
37: Also at Institute for Theoretical and Experimental Physics, Moscow, Russia
38: Also at Gaziosmanpasa University, Tokat, Turkey
39: Also at Adiyaman University, Adiyaman, Turkey
40: Also at The University of Iowa, Iowa City, USA
41: Also at Mersin University, Mersin, Turkey
42: Also at Kafkas University, Kars, Turkey
43: Also at Suleyman Demirel University, Isparta, Turkey

44: Also at Ege University, Izmir, Turkey
45: Also at School of Physics and Astronomy, University of Southampton, Southampton, United Kingdom
46: Also at INFN Sezione di Perugia; Università di Perugia, Perugia, Italy
47: Also at Utah Valley University, Orem, USA
48: Also at Institute for Nuclear Research, Moscow, Russia
49: Also at Los Alamos National Laboratory, Los Alamos, USA
50: Also at Erzincan University, Erzincan, Turkey
51: Also at Kyungpook National University, Daegu, Korea